In Vivo Determination of the Physiological and Functional Properties of Muscle Using Multi-Scale Measurements of Muscle Architecture

---

A Thesis

Presented to

the faculty of the School of Engineering and Applied Science

University of Virginia

---

in partial fulfillment
of the requirements for the degree

Master of Science

by

Evan J. Terrell

May 2018

APPROVAL SHEET

This Thesis
is submitted in partial fulfillment of the requirements
for the degree of
Master of Science

Author Signature: 

This Thesis has been read and approved by the examining committee:

Advisor: Silvia S. Blemker

Committee Member: George J. Christ

Committee Member: Joseph Hart

Committee Member: _____

Committee Member: _____

Committee Member: _____

Accepted for the School of Engineering and Applied Science:

Craig H. Benson, School of Engineering and Applied Science

May 2018

UNIVERSITY OF VIRGINIA

IN VIVO DETERMINATION OF THE PHYSIOLOGICAL AND FUNCTIONAL PROPERTIES OF MUSCLE USING MULTI-SCALE MEASUREMENTS OF MUSCLE ARCHITECTURE

A THESIS

SUBMITTED TO THE GRADUATE SCHOOL
IN PARTIAL FULLFILLMENT OF THE REQUIREMENTS

for the degree

MASTER OF SCIENCE

Field of Biomedical Engineering

By

Evan Terrell

CHARLOTTESVILLE, VIRGINIA

January 2018

ABSTRACT

IN VIVO DETERMINATION OF THE PHYSIOLOGICAL AND FUNCTIONAL PROPERTIES OF MUSCLE USING MULTI-SCALE MEASUREMENTS OF MUSCLE ARCHITECTURE

Evan Terrell

Muscle architecture, defined as the spatial arrangement of fiber bundles relative to the axis of force generation, is a critical determinant of muscle functional capacity. Computational models are routinely used in the field of biomechanics to estimate muscle force generation and simulate human movement based on architecture inputs, providing an efficient and flexible platform to study human performance, explore the effects of pathologies, and develop novel therapies. Existing muscle architecture data is limited, often coming from cadaver dissection studies, which fail to accurately represent the architecture of healthy musculature. There exists a critical need for comprehensive, accurate human muscle architecture data upon which reliable musculoskeletal models can be developed and validated. Fortunately, new *in vivo* imaging technologies now present the opportunity to address this need.

The objectives of this work were to apply a multi-scale *in vivo* imaging framework to study the architecture of the tibialis anterior (TA) muscle non-invasively in healthy adult subjects. Magnetic resonance imaging was used to measure the volume of the muscle. Ultrasound imaging was applied to explore fascicular architecture and estimate tendon moment arm. Finally, a recently developed laser-based micro-endoscopic imaging system was used to measure the length of muscle sarcomeres. Using this information, we have, for the first time, calculated the optimal fascicle length and physiological cross-sectional area (PCSA) of the TA entirely from *in vivo* measurements of muscle architecture. Operating range and force-production capacity were then estimated, allowing us to predict dorsiflexion moments produced about the ankle joint by the TA. These predictions were compared against experimentally measured dorsiflexion moments to evaluate the accuracy of architecture-based estimates. Lastly, the sensitivity of moment estimates to architecture parameter values and methodology was explored, providing an indication of the factors most critical to the development of reliable computational models.

Architecture measurements in this study agreed well with published data for the TA muscle. Dorsiflexion torque estimates derived from measured muscle architecture were found to differ significantly from measured dorsiflexion torque ($p < 0.0005$). Among the architectural parameters measured in this work, moment estimates were found to be most sensitive to variations in sarcomere length. Sensitivity of our computational approach to the cumulative effects of methodological variants and measured parameter values was more than sufficient to explain discrepancies between measured and estimated dorsiflexion moments, indicating that minor inaccuracies in architecture measurements can confound predictions of muscle function in computational models.

ACKNOWLEDGMENTS

I would like to first extend my sincerest gratitude to my principal advisor, Dr. Silvia Blemker, who taught me a great deal through her incredible insights and knowledge of muscle mechanophysiology. She was often able to find excitement in my project even when I could not, and her enthusiasm for biomechanics research is infectious. I would also like to thank her for her understanding and support as I navigated changes in my graduate education path.

I would like to thank my colleagues for their frequent assistance with experiments and their willingness to offer their knowledge, time, and experience in support of my work. Vi Tran, Adrienne Williams, and Jordan Word were especially helpful in their contributions to image data collection. Dr. Shawn Russell and Dr. Xiao Hu oversaw the collection of gait and dynamometry data for this study. Eric McVey was vital to the recruitment of subjects and the coordination of the many components of the project. Dr. David Weiss, Dr. George Christ, and Dr. Joe Hart outlined protocols and shared insight throughout the study. Thanks to Gabriel Sanchez for providing training and advice on sarcomere imaging. I am also grateful to Dr. Brian Jones, Katie Pelland, Kelley Virgilio, Katie Knaus, Hunter Wallace, Amanda Meppelink, and Ben Anton for their mentorship and valuable feedback on my work.

I was fortunate to have the support of my wonderful family and friends to help me through the many challenges of my graduate school experience. I am particularly grateful to Mom, Dad, Kelsey, Chloe, Grace, Becka, and Scooter for providing much needed encouragement and emotional support.

My graduate work has been funded in part through the National Institutes of Health Biomedical Data Science Training Grant, as well as through the Department of Defense grant W81XWH-15-C-0084 and KeraNetics LLC.

CONTENTS

FIGURES

TABLES

1 INTRODUCTION

A comprehensive understanding of skeletal muscle architecture is vital to predicting the functional capacity of individual muscles in both healthy and pathological states. Muscle architectural parameters, including fascicle length, pennation angle, moment arm, and sarcomere length are key inputs to musculoskeletal models, which are used increasingly in the field of biomechanics to simulate movement, explore the effects of disease, and guide therapeutic procedures (Delp and Loan, 2000; Steele et al., 2010, Mansouri et al., 2016). At present, available muscle architecture data upon which models can be built and validated are limited, thus compromising model performance and diminishing trust in the results of modeling studies.

Current musculoskeletal models of the human lower limb are largely built using architecture data reported from three cadaver dissection studies (Friederich and Brand, 1990; Ward et al., 2009; Wickiewicz et al., 1982). Measurements generated from cadaver studies fail to accurately represent the architecture of healthy adult musculature due to methodological challenges, demographic differences, and tissue property changes that occur post-mortem and post-fixation (Martin et al., 2001; Van Ee et al., 2000; Vidt et al., 2011). Because of these limitations, non-invasive methods are needed to explore the muscle architecture of living healthy subjects *in vivo*. Advances in musculoskeletal imaging, including magnetic resonance and ultrasound technologies, have enabled the visualization of fascicular architecture and whole-muscle morphology *in vivo*; however, a non-invasive method to study architecture at the sarcomere level has remained elusive (Handsfield et al., 2014; Maganaris, 2003). Recently, a novel micro-endoscopic imaging system has been developed, which relies on the second harmonic generation properties of myosin protein filaments to generate images of individual muscle sarcomeres *in vivo* (Sanchez et al., 2014). With this system now available, the tools exist for researchers to collect

complete human muscle architecture data across scales and to use this data to improve understanding of muscle structure-function relationships and advance musculoskeletal modeling technologies.

The objectives of this study were to (i) determine, for the first time, the optimal fascicle length and physiologic cross-sectional area of the tibialis anterior muscle entirely from *in vivo* measurements of muscle architecture, (ii) use architectural and physiological measurements to estimate functional capacity of the tibialis anterior and compare this estimate to measured torque production, and (iii) evaluate the impact of methodological considerations and parameter sensitivity on the accuracy of muscle torque estimates. The tibialis anterior (TA) was selected as the muscle of interest for this study because its large size, relatively simple structure, and superficial location within the lower limb make it conveniently accessible for *in vivo* imaging and functional assessment.

A multi-scale experimental framework was employed in this work to study the structure of the TA in five human subjects. The framework consisted of four stages: (1) magnetic resonance imaging was performed to study the morphology and size of the TA, (2) ultrasound imaging was performed to study fascicular architecture and muscle moment arm, (3) micro-endoscopic imaging was performed to collect information about sarcomere arrangement in the muscle, and (4) dynamometric testing was performed to evaluate the functional capacity of the muscle. Information derived from experimentation was used to compute key physiological properties. These properties enabled us to determine the force-length relationship of the TA, and thus allowed for an architecture-based calculation of muscle torque production. This architecture-based torque estimate was compared to dynamometric measurements, and the influence of various experimental and computational parameters on its value was assessed.

This thesis describes the methods used to collect muscle architecture data and compute functional estimates. Chapter 2 provides an overview of existing musculoskeletal biomechanics research and *in vivo* imaging techniques. It also discusses the significance of this work. Chapter 3 describes the experimental and computational methods used throughout the study. Chapter 4 presents our results, including summaries of measured muscle architectural properties and comparisons between functional estimates and measured functional data. Chapter 5 discusses the significance of our results and describes the limitations and potential future directions for this work.

2 Background and Significance

2.1 Significance of Muscle Architecture

The architecture of skeletal muscle is a critical determinant of its biomechanical capabilities. It is well-established that skeletal muscle has a highly-organized hierarchical structure. At the molecular scale, muscle is made up of sarcomeres, which are the fundamental force-producing units of the tissue. These sarcomeres are comprised of interdigitated actin and myosin protein filaments, which interact to generate tension through contractile action. Sarcomeres are connected in series to form myofibrils, which are bundled in parallel to form muscle fibers, the multi-nucleated cellular unit of muscle tissue. Fibers are then bundled in parallel groupings, which form fascicles. These parallel groupings increase the force production capability of the muscle and help to transfer loads laterally throughout the tissue. There is also evidence that fibers are connected longitudinally in a staggered, interdigitated fashion, as individual fibers often do not span the entire length of the muscle fascicles (Loeb et al., 1987). Fascicles extend from the skeletal origin of the muscle to its tendinous insertion, transferring loads to the skeletal structure and facilitating motor function (Figure 2.1).

Despite the remarkable consistency of this hierarchical structure across muscles and species, individual muscles vary from one another in regard to their architecture. Muscle architecture is defined as the arrangement of fibers within a muscle relative to the axis of force generation (Lieber and Friden, 2000). This fiber arrangement is specific to the individual muscle, and it is critical to determining how the muscle operates within the musculoskeletal system. Despite the diversity of architectural designs across human muscles, there are several architectural categories within which all muscles fall.

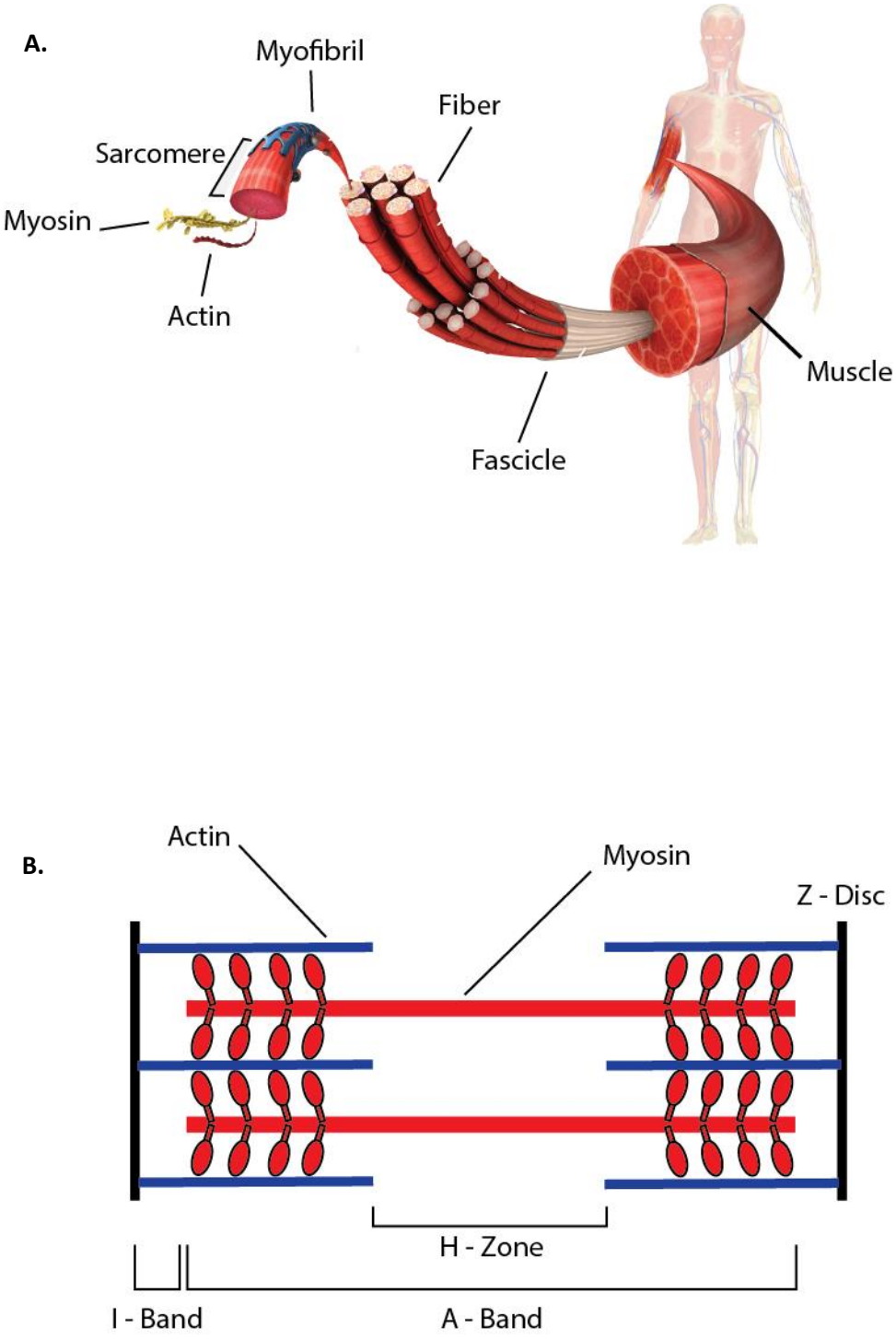

Figure 2.1. ***Structure of the Muscle and Sarcomere****. (A) The fundamental contractile unit of muscle tissue is the sarcomere, which is comprised of interdigitated actin and myosin filaments. Sarcomeres connect in series to form myofibrils, which are bundled in parallel to make up a single muscle fiber. Parallel bundles of fibers form fascicles, which form the muscle body. Figure retrieved from https://weighttraining.guide/muscle-fibers/. (B) Within the sarcomere, myosin heads interact with actin filaments to generate tension through an ATP-dependent reaction. Individual sarcomeres are separated by a protein structure called the Z-disc.*

Muscle architecture categories are summarized in Figure 2.2. The simplest category is made up of muscles with parallel fiber architecture. These muscles have fascicles that extend along a straight-line path from the origin of the muscle to its insertion. Muscles of this category tend to be long and thin with narrow regions of attachment. A unique form of parallel muscle architecture is circular architecture in which there are no skeletal attachment points and instead fascicles run in a circle. This arrangement is used to contract or expand openings of the body and is common around the mouth and sphincters. Similar to parallel architecture is fusiform architecture. Muscles with a fusiform arrangement tend to have narrow skeletal attachment points, but are wider and cylindrical within the muscle belly. Muscles with convergent, or fan-shaped fiber arrangements have one narrow and one broad attachment, with fibers following a straight-line path from origin to insertion. Dissimilar to parallel architecture is pennate architecture. Pennate muscles have fibers which span their attachment points at an angle to the axis of force generation. In unipennate muscles, all fibers are oriented at the same angle relative to the tendon line of action. Bipennate muscles contain two distinct unipennate regions, which may have symmetric or asymmetric angles of pennation. Lastly, multipennate muscles can be comprised of any number of unipennate regions. Most human muscles fall into this final category (Lieber and Friden, 2000).

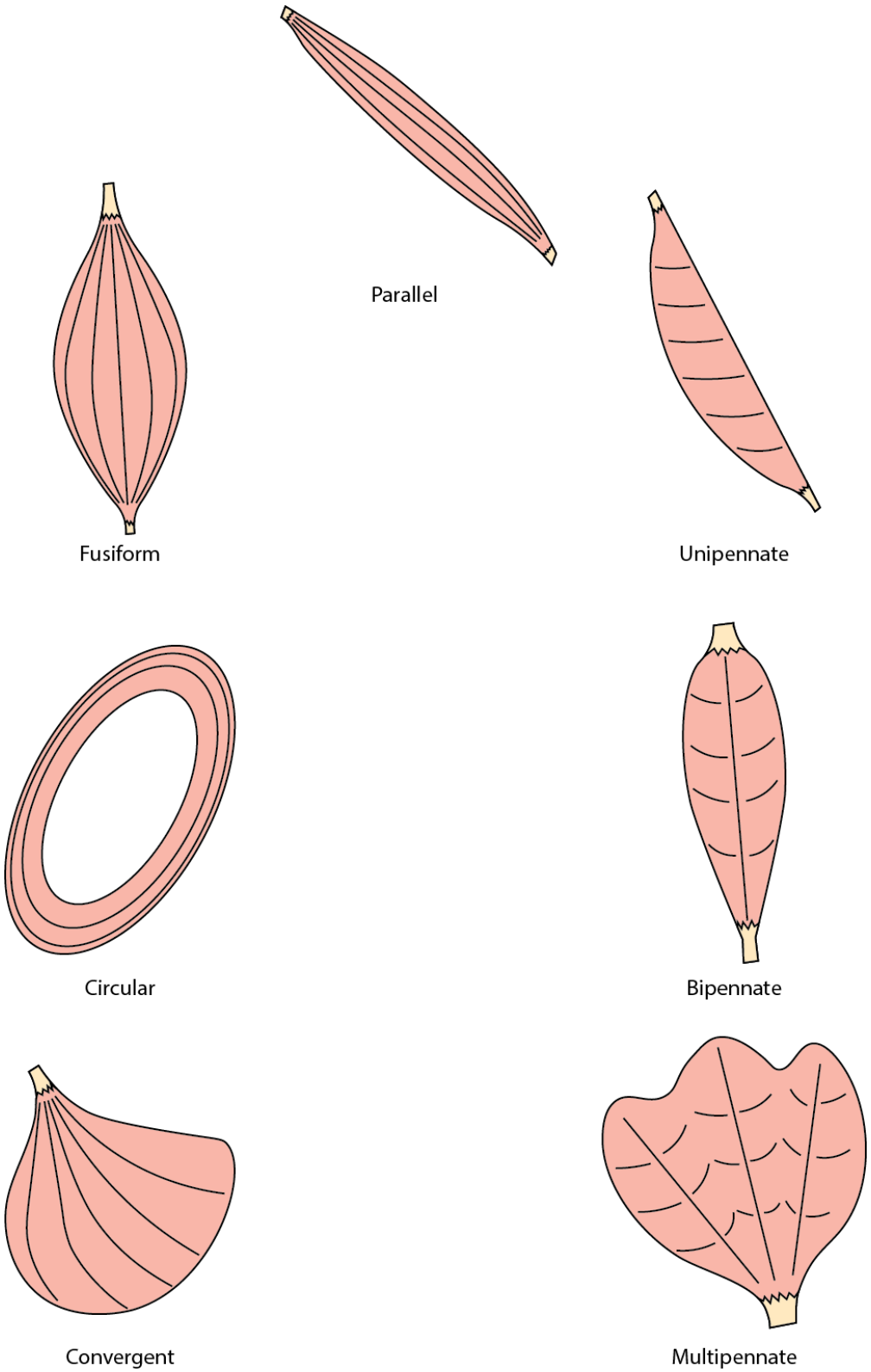

Figure 2.2. ***Muscle Architecture Types.*** *The architecture of muscles in the human body varies widely depending on the muscle's location and functional role. Common architecture types include parallel, fusiform, circular, convergent, unipennate, bipennate, and multipennate. A majority of muscles have complex architecture and thus fall into the multipennate category.*

Understanding the architectural design of individual muscles is valuable because it is this design which defines the functional properties conveyed by the muscle. The length-tension and velocity-tension relationships of sarcomeres and, thus, muscle fibers are well-established and known to be consistent across fibers of different muscle types, individuals, and species. Specifically, an optimal length for sarcomere force generation has been identified as the length at which maximum interaction between actin and myosin filaments is achieved. At shorter and longer sarcomere lengths, portions of the actin and myosin filaments are unable to interact, thus inhibiting force production. Using this information, a length-tension curve for muscle fibers has been developed (Gordon et al., 1966). Similarly, researchers have established a velocity-tension relationship for muscle, which shows a hyperbolic decrease in force capacity with increasing velocity of shortening (Figure 2.3). This relationship arises due to the rate constant of molecular cross-bridge formation between actin and myosin filaments during shortening. At low contraction speeds, more cross-bridges can form, allowing the muscle to sustain greater tensions, while at high contraction speeds, fewer cross-bridges have time to cycle properly (Hill, 1938).

Given these two fundamental relationships of skeletal muscle, knowledge of architecture for a specific muscle enables one to predict the muscle's functional role. For example, a long, thin, parallel-fibered muscle has many sarcomeres acting in series, thus allowing the muscle to operate over a broad range of lengths and achieve higher contraction velocity. Muscles of this type can traverse a large region of the length-tension curve, but produce limited force due to their lack of sarcomeres acting in parallel. These muscles often act synergistically to primary movement-producing muscles and serve to stabilize joints for fine motor control. In contrast, a thick muscle, with short, highly-pennated fibers will operate over a smaller length range and will not be able to

achieve large contraction velocities. However, the thickness and pennation of the muscle allows more sarcomeres to act in parallel, generating greater tension. It is the diverse array of muscle architectures found throughout the human musculoskeletal system that enables broad and complex motor capabilities (Lieber and Friden, 2000).

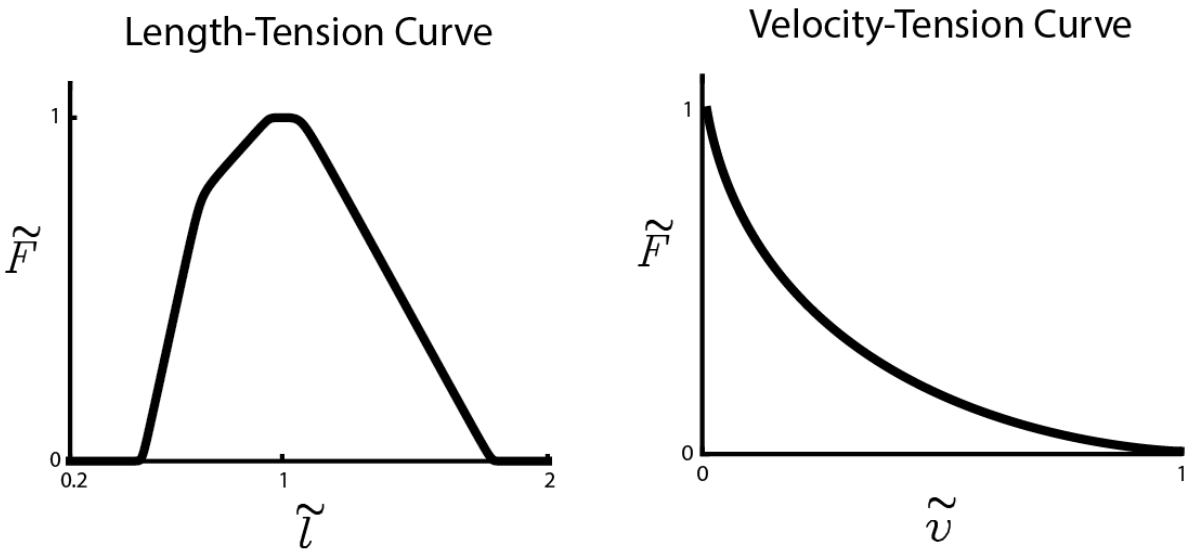

Figure 2.3. ***Muscle Length-Tension and Velocity-Tension Relationships.*** *The length-tension and velocity-tension relationships are well-established and fundamental to muscle function. The length-tension relationship of muscle states that an optimal length exists at which a given muscle can actively generate maximal force. This behavior arises due to the structure of the sarcomeres comprising muscle (Fig 2.1). The velocity-tension relationship of muscle states that a muscle can sustain maximal tension when it is isometric. The faster a muscle contracts, the less tension it can sustain. This behavior arises due to myosin-actin interactions, which are inhibited as sarcomeres shorten more rapidly.*

Several muscular properties can be measured experimentally to define the architecture of a given muscle. Fascicular architecture is generally defined by fascicle length, the length of fascicles running from one muscle-tendon junction to the other, and pennation angle, the angle of fascicles relative to the line of action of the muscle. Because these properties vary with the length of the muscle and, thus, the position of the corresponding joint(s), it is important that these properties are measured across the muscle's physiological length range. Other structural and morphological properties are also valuable in understanding how muscle architecture influences functional capacity, including muscle volume, tendon moment arm, and sarcomere length. Tendon

moment arm refers to the perpendicular distance between a muscle's path of action and the center of rotation of the joint being articulated by the muscle. Sarcomere length is the distance between consecutive sarcomere Z-disks within a muscle fiber. In this study, all the above properties are collectively termed "muscle architecture".

Researchers have developed methods to compute key physiological and functional properties using muscle architecture measurements. Optimal fascicle length (l_{fo}), which describes the length at which the sarcomeres within a muscle fascicle are at optimum length, thus allowing for maximum muscle force production, can be computed according to the following relation:

$$l_{fo} = l_f / l_s * l_{s0} \tag{2.1}$$

where l_f is the measured muscle fascicle length at a given joint position, l_s is the measured muscle sarcomere length at the same joint position, and l_{s0} is the optimal sarcomere length for human muscle. Knowledge of optimal fascicle length for a specific muscle is valuable because it allows one to determine at which region on the length-tension curve the muscle operates and, thus, the forces the muscle is able to generate relative to its maximum force potential (Chang et al., 1999; Maganaris, 2001; Zajac, 1989). Physiological cross-sectional area (PCSA) defines the area of the muscle through a cross-section plane that is perpendicular to the pennation angle of the muscle. This metric describes the number of sarcomeres acting in parallel within the muscle and is directly related to the maximum force the muscle can generate (Bamman et al., 2000; Brand et al., 1986; Fukunaga et al., 2001). It is calculated as follows:

$$PCSA = V / l_{fo} \tag{2.2}$$

where V is the measured muscle volume. Using this information, along with the measured pennation angle and moment arm of the muscle, one can estimate the moments a muscle is able to generate about its corresponding joint(s), thus allowing one to predict biomechanical function.

Studying and applying muscle architecture is fundamental to the field of biomechanics. Thus, clinical impacts of work in this area are far-reaching. Architecture-based estimates of muscle functional capacity are used heavily for biomechanical modeling and simulation. Researchers employ these simulation tools to determine the muscle actions required to achieve movements of interest and to explore the effects of disease and injury on muscle behavior and motor performance (Delp and Loan, 2000; Steele et al., 2010). Knowledge of muscle architecture is used to guide musculoskeletal therapeutic procedures, such as tendon transfer and cleft palate repair surgeries, and is also valuable in developing training protocols that improve human performance (Inouye et al., 2015; Mansouri et al., 2016). Recently, architectural data has been employed as a baseline to which researchers aim to match the properties of engineered muscle tissue constructs for the treatment of volumetric muscle loss injuries (Baker et al., 2017). Given the fundamental nature of muscle architecture information, it is critical that there exists accurate architecture data for all muscles of the human body and that models being used to predict functional properties from this data are robust and reliable.

Despite its importance and long history of study, our knowledge of human muscle architecture remains limited. Previous studies have relied on cadaveric specimens for data collection. Wickiewicz et al. (1983) generated a comprehensive muscle architecture dataset for human plantarflexors and dorsiflexors; however, only three cadaveric specimens were used in their study, thus bringing the reliability of their results into question. Similar concerns exist regarding the results of Friederich and Brand's 1990 work, in which lower limb muscle architecture was measured from two cadaver specimens. Ward et al. (2009) undertook a similar cadaver-based study of lower limb muscle architecture using 21 specimens.

The results of these studies have been widely used in computational models of lower limb biomechanics since publication, but recent findings have brought these works under scrutiny by identifying differences in muscle architecture between cadaver specimens and healthy adults. For example, Friederich and Brand (1990) discuss limitations to cadaveric architecture studies, including small sample sizes and "uncontrollable and unpredictable" shrinking of dissected fascicles. Martin et al. (2001) compared gastrocnemius and soleus architecture measured from 5 cadaver specimens to that measured *in vivo* via ultrasonographic imaging of 9 healthy subjects. They found significant differences in fascicle length and pennation angle between the cadaveric and *in vivo* measurements in both the gastrocnemius and soleus, with fascicle length differences as high as 21.1% and pennation angle differences as high as 179.4%. Van Ee et al. (2000) measured changes in muscle tissue mechanical properties of cadavers with post-mortem time and freezing. Their research revealed significant changes in muscle tissue elastic modulus after 8 hours post-mortem, as well as a significant decrease in failure stress and failure energy of 61% and 81%, respectively, compared to healthy tissue samples. Finally, Vidt et al. (2011) used magnetic resonance imaging (MRI) to study the effects of aging on upper extremity muscle volumes, finding that muscle volumes are significantly lower in elderly adults compared to young adults. Because cadaver donors are most often elderly adults, architecture measurements from cadaveric specimens are not representative of healthy adult populations.

Although *in vivo* methods to study muscle architecture, including MRI and ultrasound, have been developed and are widely used in the field of biomechanics, there has yet to be a comprehensive muscle architecture dataset created entirely from *in vivo* methods. Until recently, a non-invasive method to measure muscle sarcomere lengths *in vivo* was not available, which prevented progress in this area. However, new technology has now made *in vivo* sarcomere

imaging a reality, thus providing new opportunities to generate accurate and comprehensive human muscle architecture data.

2.2 Measuring Muscle Architecture

Historically, human muscle architecture has been studied through cadaver dissections. In these studies, muscles of interest are first surgically exposed. Pennation angle is then measured manually using a goniometer or compass with the muscle in its *in situ* position or after removal from the body. Muscle volume is measured via fluid displacement or estimated from the mass of the muscle using a known density of 1.05 kg/cm^3. Individual muscle fiber bundles are then isolated through manual dissection and/or dissolving the tissue in media. A sampling of fiber bundles from various locations throughout the muscle is then measured manually to determine fascicle length. Measurement of sarcomere lengths have been neglected in several past muscle architecture studies. When reported, sarcomere lengths are generally measured through microscopy or laser diffraction techniques (Ward et al., 2009).

In addition to the problems associated with cadaveric architecture studies described above, several methodological limitations exist. First, architecture properties reported in these studies are often only measured for the most superficial fiber bundles, as these are the most accessible during dissection. Furthermore, because the muscle is removed from its anatomical position for measurement, the true *in vivo* configuration of muscle fibers remains unknown. Cadaver specimens do not allow for architecture measurements across a joint range of motion, and they do not allow for comparisons between measurements taken in the passive and active state of the muscle. Finally, without accurate, *in vivo* sarcomere length measurements, the reported lengths of fascicles are meaningless because fascicle length relative to optimal is not known. Clearly, it is advantageous to measure muscle architecture using non-invasive *in vivo* techniques in which

measurements can be made under various physiological conditions without disrupting anatomical structure or positioning. Fortunately, the last few decades have seen a rise in *in vivo* musculoskeletal imaging techniques, making non-invasive measurements of muscle architecture a reality.

In recent years, computed tomography (CT) and MRI have become the "gold-standard" approaches to measuring muscle volume, with MRI being preferred due to its limited radiation exposure. Both modalities generate a series of planar images of the muscle in cross section. Volume measurements are derived from these images using manual or software-based segmentation techniques, in which the outer boundary of the muscle is delineated and the area of the boundary determined. Each cross-sectional area (CSA) is multiplied with the image slice spacing and summed, providing an estimate of muscle volume. Engstrom et al. (1991) compared the accuracy of muscle CSA measurements made using MRI and CT to those made manually using three cadaver specimens. They found that both MRI and CT CSA measurements correlated extremely well with manual measurements, with correlation coefficients of 0.99 and 0.98, respectively. This indicates that both MRI and CT are reliable methods for measuring the area of muscle cross sections. Mitsiopoulos et al. (1998) performed a similar study in which MRI and CT-based muscle volume measurements were compared to cadaver-derived measurements from two cadaver specimens. No significant difference was found between the MRI, CT, and cadaver approaches ($p > 0.01$).

Since the accuracy of these methods has been confirmed, they have been used extensively in the field of biomechanics. Narici et al. (2003) and Vidt et al. (2012) both used MRI to study the effects of aging on muscle size. Fukunaga et al. (2001) performed MR imaging and dynamometric testing on the upper extremities of 259 athletes and healthy controls to identify significant

correlations between muscle volume and joint torque ($r = 0.783$). Handsfield et al. (2014) used MRI to quantify muscle volume in 35 lower limb muscles of 24 subjects, discovering that muscle volume correlates strongly with the product of body mass and height ($r^2 = 0.92$).

To avoid the challenges associated with cadaver-based fascicular architecture measurements, standard B-mode ultrasonography is now commonly used to visualize fascicles *in vivo*. For example, Maganaris (2003) utilized ultrasound imaging to explore the length-tension relationship of the gastrocnemius muscle *in vivo*; however, his findings were limited by an inability to also measure sarcomere lengths. Several studies have aimed to elucidate the changes in architecture that take place during muscle contraction, finding that pennation angle increases and fascicle length decreases with increasing activation (Fukunaga et al., 1997; Hodges et al., 2003; Maganaris and Baltzopoulos, 1999). Other studies have used ultrasound to identify architectural differences between healthy and clinical populations. Narici et al. (2003) found that fascicle length and pennation angle in the gastrocnemius are smaller by 10.2% ($p < 0.01$) and 13.2% ($p < 0.01$), respectively, in elderly subjects compared to healthy controls. Kawakami et al. (1993) demonstrated that fascicle pennation angles in the triceps brachii are significantly larger ($p < 0.01$) in body builders than in untrained controls. The large number of publications using ultrasound to study muscle architecture supports the modality's utility for this application.

Despite its prevalence, ultrasound imaging of muscle architecture is not without limitations. Ultrasonography generates only planar images, which may not be sufficient to capture the complex spatial arrangements of many muscle fascicles (Blemker et al., 2007). Furthermore, ultrasound-based measurements have been demonstrated to be sensitive to probe positioning, with significant differences found between fascicle length and muscle thickness measurements from the same anatomy using different ultrasound probe orientations (Klimstra et al., 2007). An alternative

approach involves the use of diffusion tensor MR imaging (DTMRI). DTMRI uses MR techniques to quantify the diffusion anisotropy of water through muscle tissue. Because water will diffuse more readily along the path of a muscle fiber relative to a perpendicular path, DTMRI provides fiber trajectory information at each point in the muscle tissue and can be used to visualize and measure complex fiber arrangements (Heemskerk and Damon, 2007).

Previous cadaver-based studies of muscle architecture generally fail to report muscle moment arms, and, given the differences between cadaver specimens and healthy musculature, even those studies that do measure moment arms likely are not reporting measurements representative of healthy physiology. There are two primary approaches to measuring muscle moment arms using *in vivo* imaging. One approach involves the use ultrasound to measure the displacement of the muscle-tendon junction for a given joint rotation and to compute moment arm (R) via the tendon-excursion relation:

$$R = \frac{dx}{d\theta} \tag{2.3}$$

where x represents the displacement of the muscle-tendon junction, and θ represents the joint angle throughout joint rotation. The theoretical basis for the tendon-excursion approach to moment arm calculation is the principle of virtual work. For the muscle-tendon system to satisfy this principle, it is assumed that no stretch occurs in the tendon during joint rotation. The validity of this assumption has been called into question, particularly for moment arm measurements made in the active state. The accuracy of this approach, as well as the sensitivity of muscle function estimates to moment arm measurements, are explored throughout this work.

Alternatively, moment arm can be measured *in vivo* using MRI. In the past, a geometric approach has been used in which 2D MR images are taken with the joint of interest at two different positions. By noting the change in position of anatomical landmarks between the two joint

positions, the joint center of rotation can be determined and the perpendicular distance between this point and the tendon of interest can be measured. This approach is not without limitations, as it is restricted to 2D visualization, which is often insufficient to accurately determine the center of rotation of joints with complex 3D articulations. However, progress has been made in developing 3D, dynamic MRI methods that allow for accurate and continuous moment arm estimation across a joint range of motion (Clarke et al., 2015).

Both ultrasound and MRI have been used extensively to measure muscle moment arms. Ito et al. (1999) used ultrasound to measure moment arms of the tibialis anterior muscle via tendon excursion under three different levels of muscle activation (0, 30, and 60% maximal), finding that moment arms measured under no muscle activation (0%) were significantly smaller than those measured under 30% and 60% activation. Rugg et al. (1990) used the MRI-based center of rotation method to measure the moment arms of both the Achilles tendon and TA in 10 subjects, reporting that Achilles tendon moment arm increased 20% and TA moment arm decreased 30% when the ankle joint was moved from maximum dorsiflexion to maximum plantarflexion. Several studies have compared ultrasound and MRI moment arm measurements for the same subjects. Maganaris (1999) compared TA moment arm measurements between the two methods, finding the measurements to be comparable in the resting state. However, the MRI-based measurement was significantly smaller when the muscle was maximally active compared to resting ($p < 0.05$), while the results of the ultrasound-based measurement did not change significantly with activation. A similar result was found when comparing the results of the two methods for the Achilles tendon (Maganaris and Baltzopoulos, 2000).

Until recently, no non-invasive method to measure sarcomere lengths *in vivo* was available. Historically, sarcomere lengths were measured *ex vivo* and/or *in situ* using traditional microscopy

techniques or laser diffraction. Sarcomeres can be visualized and measured using various standard microscopy modalities, including bright field and confocal microscopy. However, this generally requires that a biopsy be taken from the muscle of interest to allow for loading onto the microscope stage (Ward et al., 2009). Alternatively, the laser diffraction technique allows one to estimate sarcomere width by measuring the diffraction pattern that is created when laser light is shone through the muscle fibers. In this case, the sarcomeres themselves serve as a slit grating that causes diffraction of incident laser light. By measuring the spacing between consecutive constructive interference points in the resulting diffraction pattern, one can calculate the width of an individual sarcomere (Lieber et al., 1984; Cutts, 1988). Laser diffraction can be performed on an excised muscle tissue sample, as well as on a muscle in its anatomical position; however, in the latter case, the muscle must be exposed surgically, making the process highly invasive and unrepresentative of undisturbed physiology (Koolmees at al., 1986; Lieber et al., 1994; Lieber et al., 1997).

More recently, imaging methods designed around muscle tissue's intrinsic second harmonic generation (SHG) properties have been developed. SHG is a physical phenomenon in which high-intensity photons incident on surfaces with non-linear optical structure "combine", leading to a doubling of frequency and halving of wavelength (Figure 2.4). Imaging systems can detect this high-frequency light to visualize the SHG-capable material that gave rise to it. The SHG properties of muscle tissue were elucidated in 2006 when Plotnikov et al. determined that myosin filaments within muscle sarcomeres are responsible for frequency-doubling interactions. Taking advantage of these unique optical properties of muscle tissue, SHG microscopy systems have been used to measure sarcomere lengths in muscle samples *ex vivo* (Boulesteix et al., 2004). However, *in vivo* sarcomere imaging has remained elusive.

Fortunately, advances in micro-endoscopic imaging technology have given rise to a novel, minimally-invasive imaging system that relies on the SHG properties of muscle sarcomeres to image the molecular structure of muscle tissue *in vivo*. The system, developed by Sanchez et al. (2014) and now commercialized by Zebra Medical Technologies (Mountain View, CA), uses fiber optic cables to deliver high-intensity laser light to a moveable hand-held microscope. Light is transmitted from the microscope through a 20-gauge micro-engineered optical needle and directly into the musculature. There the light interacts with sarcomeres in the surrounding fibers, giving rise to SHG behavior. The resulting high-frequency light is returned to a collector through the optical needle and fiber optic cable where it is used to generate images of sarcomere arrangement.

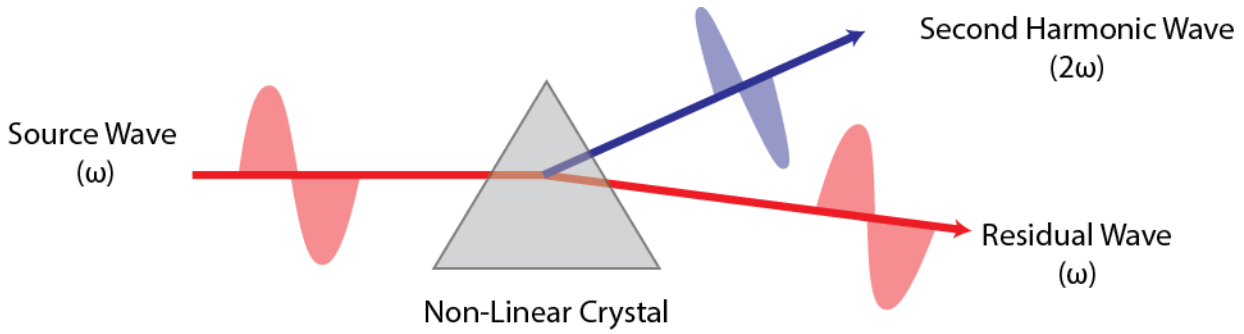

Figure 2.4. ***Second Harmonic Generation.*** *Second harmonic generation is a physical phenomenon in which high-intensity light incident on a non-linear crystal will undergo a "frequency-doubling" interaction. This creates a second harmonic wave with twice the frequency of the source wave, which can be detected to generate images of the non-linear crystal material that gave rise to the behavior. This technique is used to image sarcomeres in muscle tissue, as myosin has second harmonic generating properties.*

The use of micro-endoscopic SHG technology for *in vivo* sarcomere imaging was first introduced in 2008 when Llewellyn et al. demonstrated its ability to generate reliable measurements of sarcomere length across joint positions and to visualize twitch dynamics of individual sarcomeres in mice and humans. Sanchez et al. (2015) used the technology to detect abnormal sarcomere lengths and involuntary sarcomere twitch dynamics in the soleus muscle of post-stroke patients. Chen et al. (2016) applied the system to measure sarcomere lengths of the

vastus lateralis at a range of knee flexion angles, demonstrating the ability to estimate the length-tension behavior of the muscle across its physiological range of motion using data generated by the technology. The micro-endoscopic sarcomere imaging systems presents valuable new opportunities for improved study of muscle architecture and a better understanding of the structure-function relationships that exist across the human musculoskeletal system.

2.3 Significance of This Study

As modeling and simulation technologies continue to permeate into the field of biomechanics, the need for comprehensive muscle architecture data, upon which reliable computational models can be built and validated, has become increasingly urgent. Equally vital is a thorough understanding of the present limitations of *in vivo* methods used to study muscle architecture and the sensitivity of current computational frameworks to experimentally-derived architectural inputs. This understanding remains incomplete, though it has received some attention. Brand et al. (1986) used a non-linear optimization model and previously published muscle PCSA data to evaluate the effects of varying PCSA on muscle and joint force estimates in a kinematic model, finding that individual muscle force predictions varied by as much as 800% with varying PCSA, although total joint force estimates varied by less than 11% on average. Myers et al. (2015) performed Monte Carlo simulations within the OpenSim musculoskeletal simulation platform to assess the effects of kinematic and architectural measurement uncertainty on model performance. They found that variability in reported muscle architecture led to force predictions with 95% confidence intervals as large as 120 N. These studies, however, fail to investigate the sensitivity of functional predictions to individual architectural parameter values. They also do not consider the impact of common experimental and computational methodology variants on predicted muscle performance.

We have employed a multi-scale *in vivo* imaging framework to collect comprehensive muscle architecture data from the tibialis anterior of five healthy adult subjects. This data was used to compute the functional properties of the muscle, including optimal fascicle length, PCSA, and muscle operating range. We were then able to estimate the peak dorsiflexion torque generated by the TA across the ankle joint and compare this result with measured peak dorsiflexion moments for each subject to assess agreement between computational predictions and experimental measurements. Finally, we have explored the sensitivity of our computational approach to methodological decisions and architecture parameter values to identify the factors that are most likely to confound architecture-based estimates of muscle function. To our knowledge, this study is the first in which comprehensive architectural information, including sarcomere lengths, has been measured *in vivo* in human subjects and used to evaluate the influence of parameter measurements on computational estimates of muscle function.

3 METHODS

Complete muscle architectural and functional measurements were collected from five human subjects (m/f: 3/2, age: 33.6 ± 11.1 years, height: 173.0 ± 12.8 *cm*, body mass: 75.3 ± 23.6 *kg*). Individual subject data are summarized in Table 3.1. All subjects were healthy adults with no history of lower limb injury. Subject selection and study protocol were approved by the University of Virginia's Institutional Review Board.

Subject	Sex	Age (years)	Height (cm)	Mass (kg)	Dominant Leg
Subject 1	M	40	182.9	63.5	Right
Subject 2	F	20	157.5	59.0	Right
Subject 3	M	23	177.8	77.1	Right
Subject 4	M	42	185.4	115.7	Right
Subject 5	F	43	161.3	61.2	Right

Table 3.1. ***Subject Data.*** *Sex, age, height, mass and dominant leg are reported for the five subjects included in this study.*

The tibialis anterior (TA), an ankle dorsiflexor, was the primary muscle of interest in this study. The TA was selected because it is a relatively simple muscle with well-established bipennate architecture that only acts across a single joint. It is relatively large and superficially positioned in the lower limb, making it conveniently accessible during experimentation.

In order to develop a comprehensive understanding of muscle architecture across length scales, as well as explore voluntary functional capacity, an experimental protocol consisting of five different stages was followed. Stage one involved the determination of muscle volume from MR images of the TA. Stage two involved the collection of fascicular architecture data, including fascicle length and pennation angle, using ultrasound imaging. In stage three, tendon moment arm

was estimated using a tendon excursion approach. Stage four involved the use of micro-endoscopic imaging to measure the arrangement of sarcomeres within the musculature. Finally, in stage five, dynamometry was used to evaluate the functional capacity of the TA about the ankle joint. Experimental stages were performed at least 24 hours apart with the exception of stages two through four, which were all performed on the same day (Figure 3.1).

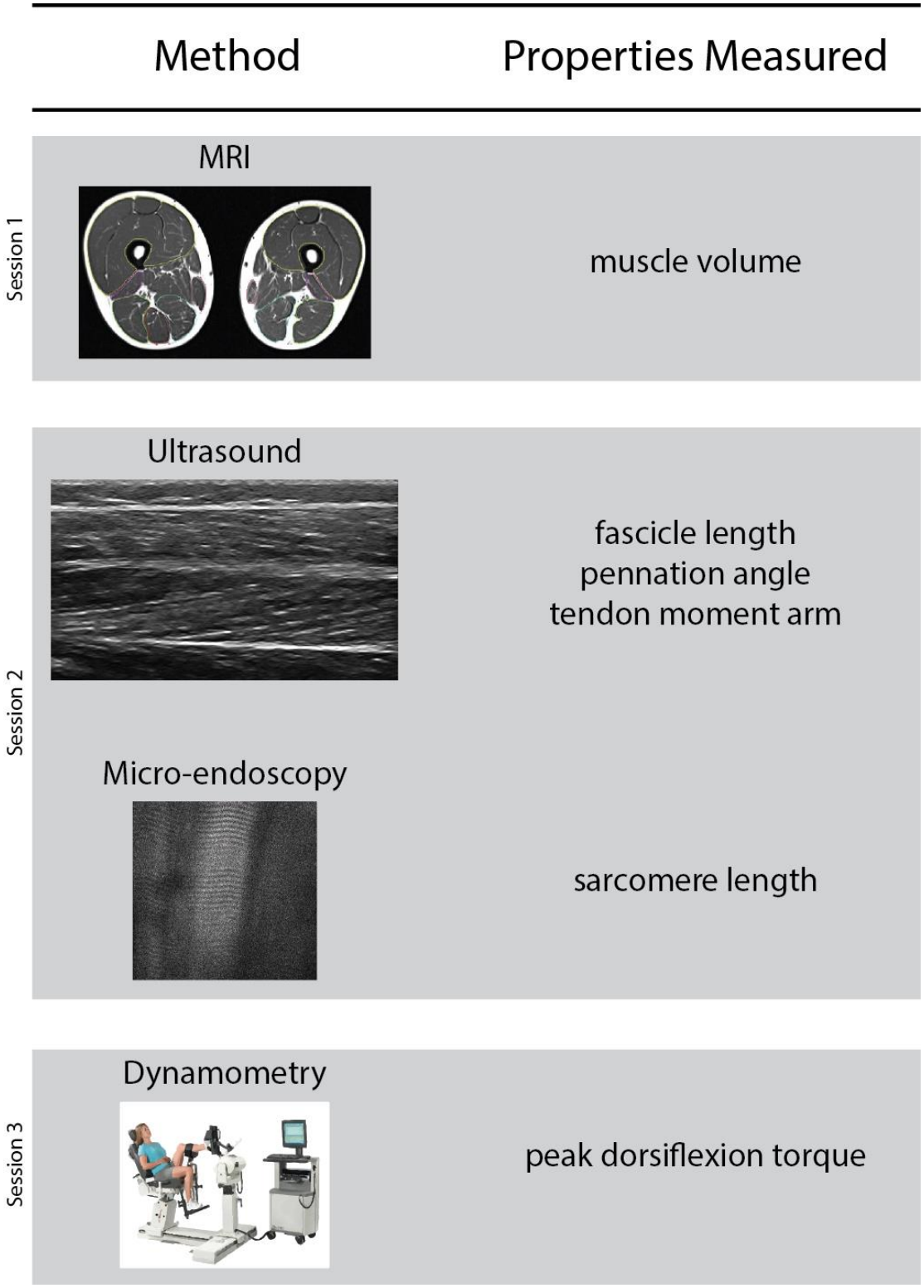

Figure 3.1. ***Methods Summary.*** *Four different in vivo data-collection modalities were used throughout this study, including: MRI, ultrasound, micro-endoscopy, and dynamometry. MRI was used to generate muscle volume data. Ultrasound was used to collect fascicular architecture and moment arm data. Micro-endoscopy was employed to image muscle sarcomere lengths. Lastly, dynamometry was used to measure torque generation of the TA muscle. Data collection occurred in three sessions, with each session taking place at least 24 hours apart. Ultrasound and micro-endoscopic imaging were performed during the same session.*

3.1 MR Imaging and Measuring Muscle Volume

MR images were collected using a 3T Siemens (Munich, Germany) Trio MRI Scanner with a 2D multi-slice sequence involving spiral gradient echo for optimal visualization of muscle tissue (Handsfield et al., 2014; Meyer et al., 1992). Axial images were collected from the iliac crest through the ankle of each subject at a slice thickness of 5 mm. Scan parameters were as follows: TE = 3.8 ms, TR = 800 ms, $\alpha = 90°$, field of view = 400 mm x 400 mm, in-plane spatial resolution = 1.1 mm x 1.1 mm. Total scan time was approximately 45 minutes. All MRI scans were performed and monitored by a trained MRI technician at the University of Virginia.

Following MR image collection, image stacks were exported to a custom musculoskeletal segmentation software developed in Matlab (Mathworks, Natick, MA). In each image frame, the boundary of the TA muscle on the subject's dominant leg was identified. A contour denoting the outer edge of the muscle was created within the segmentation software by placing a series of points connected by spline curves along the identified boundary. Axial contours were then interpolated longitudinally to generate a 3D surface rendering of the muscle (Figure 3.2). The volume of each 3D surface model was computed by multiplying the cross-sectional area of each slice contour by the slice thickness (5 mm) and summing these individual slice volumes across the entire muscle length.

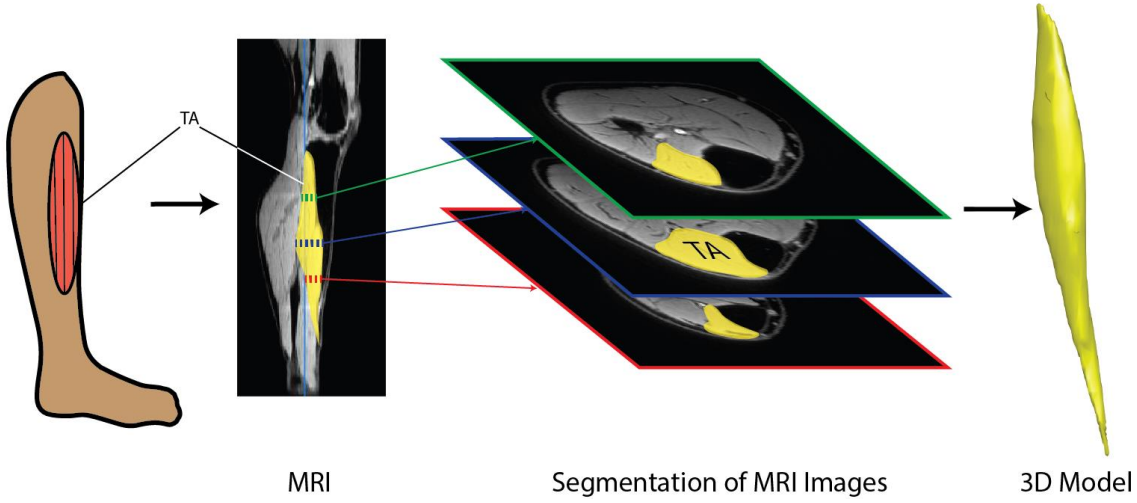

Figure 3.2. ***Magnetic Resonance Imaging.*** *MRI was used to image whole-muscle morphology. Series axial MRI images were collected at the lower limb of each subject. The TA was identified and its boundary segmented in each image slice. The segmented contours of the muscle were used to generate a 3D model from which muscle volume was measured.*

3.2 Ultrasound Imaging and Measuring Fascicle Architecture

Standard B-mode ultrasound was used to image the fascicular architecture of the TA muscle (Maganaris, 2003). Ultrasound images were collected using a Telemed (Vilnius, Lithuania) LS128 CEXT system. A 7.5 MHz veterinary ultrasound transducer was chosen for our application because its 60 mm long interface enabled a wider viewing area in collected images, thus avoiding inaccuracies in architectural measurements associated with extrapolation of muscle features beyond the boundaries of the image frame. Imaging parameters were adjusted to achieve a penetration depth of 50 mm and an image focus of 13 mm. A dynamic range of 80 dB was used. These parameters were maintained across ultrasound scans and subjects.

Imaging took place at the thickest point of the muscle belly, approximated as one third the distance from the lateral tibial condyle to the medial malleolus along the muscle path. Collecting images at this location was desirable, as this is where muscle architectural features are most clearly visible. It also ensured that the needle probe used during micro-endoscopic imaging did not

penetrate through the TA into any other anatomy during insertion. During imaging, the ultrasound probe was oriented such that its long axis aligned with the line of action of the muscle, thus generating images of the muscle cross section in the sagittal plane. The transducer was manually held at the desired position by an experimenter. An aqueous gel was used to ensure acoustic coupling and to limit deformation of the tissue due to pressure applied by the transducer.

Ultrasound images were collected with the subject's ankle held securely at four different joint angles: 10° dorsiflexion, neutral, 10° plantarflexion, and 20° plantarflexion. These joint angles were maintained during imaging using a custom brace. The brace consisted of a standard ankle orthopedic boot with hinges at the ankle joint. These hinges allowed for dorsiflexion-plantarflexion movement of the ankle within the brace and could be locked at various positions of ankle flexion. The hinges were marked to indicate ankle angles of interest, and a handheld goniometer was used to confirm that denoted brace positions agreed with true subject joint positions. The TA was imaged under two different muscle activation conditions: with the muscle at rest and with the subject sustaining a maximum voluntary contraction (MVC). For each condition, three still-frame ultrasound images were captured.

The architectural properties measured from the ultrasound images were fascicle length and pennation angle. Fascicle length was measured as the straight-line distance between the central aponeurosis of the muscle and the outer fascia along the visible fascicle paths. Pennation angle was measured as the angle between the central aponeurosis and the path of the identified fascicles. Because the TA is a bipennate muscle, these properties can be measured in both the superficial and the deep unipennate regions. Three visible fascicles were identified in each region for each collected image, and fascicle length and pennation angle were determined. All measurements were made using ImageJ software (National Institutes of Health, Bethesda, MD). Thus, a total of six

measurements were made for each architectural property in a single image, and three images were collected at each joint angle. The reported fascicle lengths and pennation angles for each subject were thus the average of the eighteen measurements taken at each joint angle (Figure 3.3).

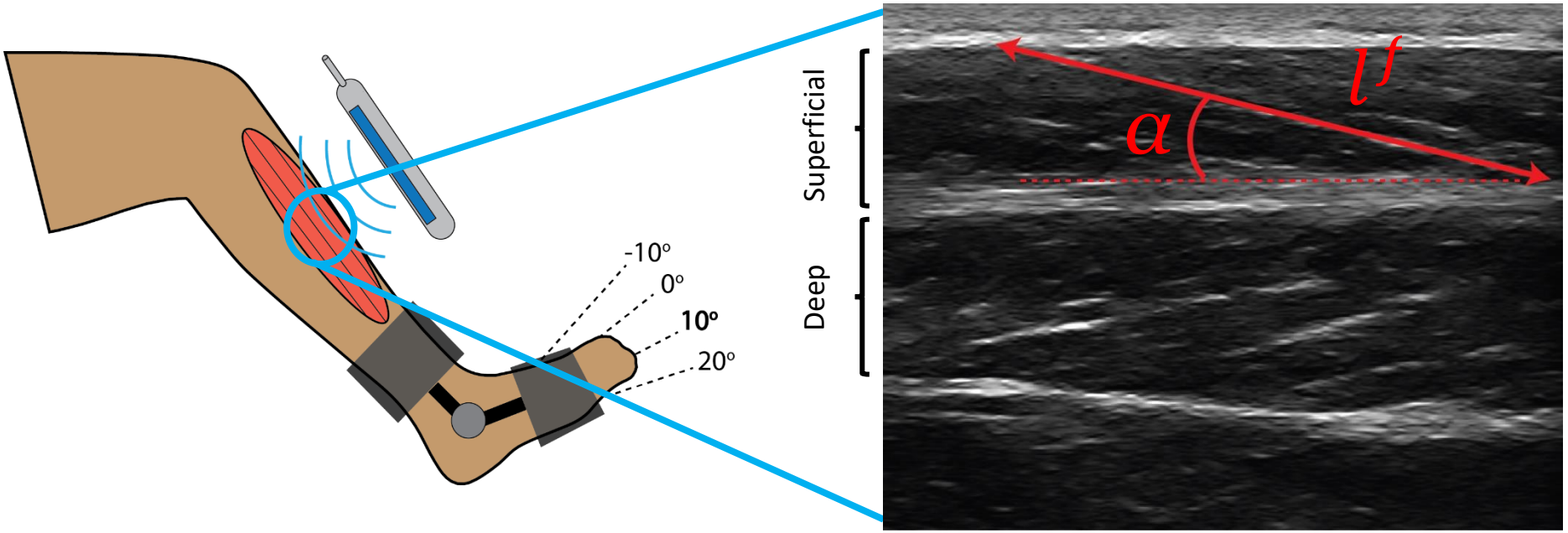

Figure 3.3. ***Measuring Fascicular Architecture Using Ultrasound Imaging.*** *Ultrasound imaging was used to visualize and measure the fascicle length and pennation angle of the TA. Images were collected at four joint angles: -10°, 0°, 10°, and 20°; and under two activation conditions: at rest and near maximally active. Fascicle length was measured as the straight-line distance from the outer fascia to the central aponeurosis along a visible fascicle path. Pennation angle was measured as the angle between the visible fascicle path and the central aponeurosis. Measurements were taken in both the superficial and deep unipennate regions of the TA and averaged to generate a single representative architecture measurement at each joint angle and each activation condition.*

3.3 Tendon Excursion Method and Computing Moment Arm

Once ultrasound imaging of fascicular architecture was completed, a tendon excursion approach was applied to compute the tendon moment arm of the TA from CINE ultrasound recordings (Ito et al., 2000). The tendon excursion method states that the moment arm of a tendon about a joint is equal to the ratio of the excursion of the tendon during a given motion of the joint to the change in joint angle during said motion. The tendon excursion method is based on the principle of virtual work, which assumes that no work is done on the tendon during joint rotation. The validity of this assumption is debated, as the development of passive tension in the tendon at large joint rotations may lead to an underestimation of moment arm. However, the tendon excursion method has been shown to agree well with other methods of TA moment arm measurement and thus is believed to be a reliable approach.

Excursion of the TA tendon was measured using CINE ultrasound imaging. The ultrasound transducer was placed again at the thickest portion of the TA muscle belly, and the long axis of the transducer again aligned with the line of action of the muscle. During image acquisition, an experimenter manually moved the subject's ankle through its passive range of motion, from peak dorsiflexion to peak plantarflexion, at a rate of ~20° per second. CINE images were collected at 20 frames per second, thus capturing displacement of the central aponeurosis of the TA during passive extension of the ankle. The ankle joint angles corresponding to peak dorsiflexion and peak plantarflexion were also measured and recorded using a handheld goniometer.

Instantaneous ankle angle was determined for each CINE recording of each subject by generating a generic curve of ankle angle over time for the passive motion described and then fitting that generic curve to the range of motion for the given subject and the timing of the given CINE recording. To do this, videos were recorded of six passive ankle extensions for a single

subject. In this case, recordings of subject 3's passive ankle motion were used to generate the generic ankle motion curve, as it was at that point in the study that the collection of this data was determined to be important. After recording, the portion of each video corresponding to the point immediately prior to the start of motion until the point immediately after the completion of motion was isolated. For each of the six passive ankle motion videos, the angle of the ankle in the sagittal plane was measured manually in each frame using ImageJ software (NIH, Bethesda, MD). This resulted in six datasets of ankle angle versus video frame number. Each of these datasets was then normalized between zero and one along both the frame number axis and the ankle angle axis, thus producing generic ankle joint motion information, which could be fit to the specifications of each subject and CINE video recording. This fitting involved scaling data along the ankle angle axis such that its initial value was the measured peak dorsiflexion joint angle and its final value was the measured peak plantarflexion joint angle for a given subject. Data was scaled along the frame number axis such that it fell within the time points at which passive ankle motion began and ended for a collected CINE ultrasound recording. Finally, a seventh order polynomial was fit to the subject-specific, recording-specific data, yielding a single curve defining a subject's instantaneous ankle angle over time.

TA tendon excursion was measured by manually tracking the position of a feature of interest on the central aponeurosis during passive ankle motion for each CINE recording in ImageJ. To compute TA moment arm, the cumulative displacement of the central aponeurosis in each ultrasound image frame was first determined by calculating the Euclidian distance between the position of the track feature in the given frame and its position in the first frame. Instantaneous joint angle was then determined by making the general motion data subject-specific and fitting a 7^{th} order polynomial. Finally, tendon displacement was plotted against ankle joint angle and a

polynomial curve was fit to the data. Initially, a second order polynomial fit curve was used, though the effects of using a third order polynomial fit are explored later in this study. The first derivative of the polynomial was analytically determined, resulting in a lower order polynomial describing TA moment arm with respect to joint angle. Using this polynomial, TA moment arm was computed at each joint angle of interest (Figure 3.4).

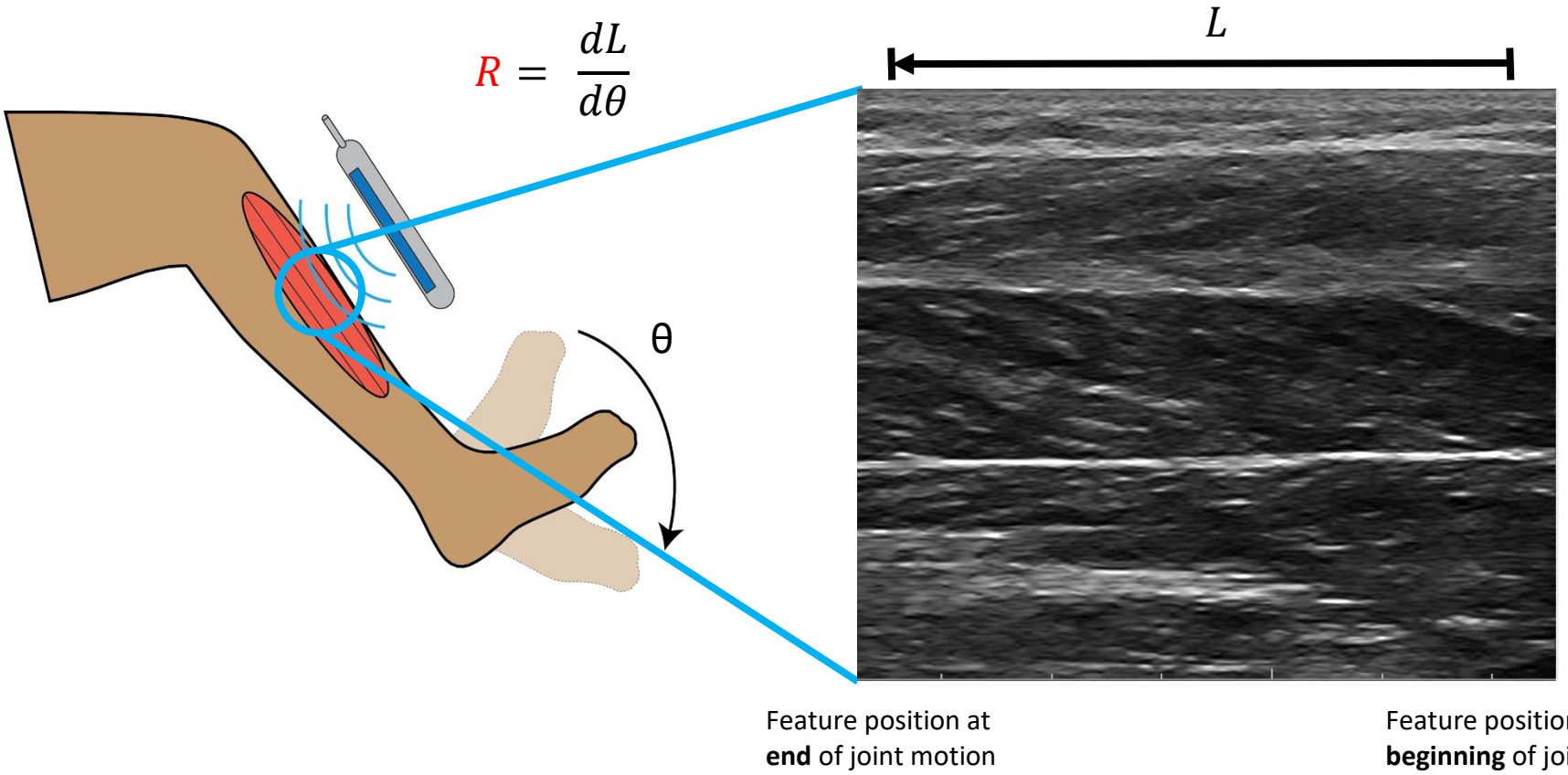

Figure 3.4. ***Measuring Moment Arm Using the Tendon-Excursion Method.*** *The moment arm of the TA was determined using the tendon-excursion method. CINE ultrasound recordings were collected while the ankle joint was passively moved through its range of motion. The displacement of a feature on the muscle-tendon junction was tracked in the resulting video and plotted against joint angle. A polynomial was fit to the tendon displacement-joint position data, and moment arm was calculated by differentiating this fit curve at each joint position of interest.*

3.4 Micro-endoscopy and Measuring Sarcomere Length

Historically, *in vivo* imaging of human muscle sarcomeres has been limited to highly invasive procedures, which modify tissue physiology and require the use of local or general anesthesia, and, thus, are limited in accuracy. Fortunately, a novel micro-endoscopic imaging system (Zebra Medical Technologies, Mountain View, CA) has been developed for non-invasive *in vivo* imaging of sarcomeres in human muscle using a physical property of myosin known as second harmonic generation (SHG). SHG is a phenomenon in which high-intensity photons incident on certain crystalline surfaces will combine to produce photons with twice the frequency and half the wavelength of the initial photons. Materials that are centrosymmetric but have planar features at the scale of photon interaction are also capable of producing an SHG signal in response to high-intensity laser light. Biological materials of this nature include collagen, and most notably for the present study, myosin (Plotnikov et al, 2006).

Leveraging the SHG properties of the myosin molecules within muscle sarcomeres, the micro-endoscopic imaging system delivers femtosecond pulses of laser light directly to the muscle tissue through a needle-based probe. Specifically, optical fibers carry light from a 1030 nm ytterbium laser to a micro-electromechanical scanning mirror, which produces the 200 fs laser scanning pattern. This light is then delivered to a dichroic mirror, which directs the light down the needle probe, where it exits via a micro-prism lens into the muscle tissue. SHG signal generated by the muscle sarcomeres is returned via the same micro-prism lens and transmitted up the needle probe and through the dichroic mirror to a photomultiplier (Sanchez et al., 2015).

Sarcomere imaging was performed at an ankle angle of 20° plantarflexion, which was maintained using the same custom brace described previously. Prior to endoscopic probe insertion, ultrasound imaging was used to identify the line of action of the TA at the position of the thickest

region of the muscle belly. The line of action was marked on the subject's skin to guide needle insertion. A spring-loaded insertion tool was used to propel the probe through the skin and into the muscle such that the two hypodermic needles located on the probe are aligned perpendicularly to the muscle fascicle direction.

Images were collected at a rate of 0.47 seconds per 512 x 512 pixel frame. The optical resolution of collected images was 1.47 μm, resulting in a field of view of 78 x 78 μm. The micro-endoscope probe was manually held in place by one experimenter while another experimenter adjusted the system properties to improve image quality and monitored the system display. If sarcomeres were not readily apparent at the initial needle insertion position, the needle was repositioned through very small translations or rotations of the probe. These movements were small enough to avoid significant deformation of the tissue surrounding the needle and to minimize patient discomfort. Once sarcomeres were identified at a given needle position, that position was maintained while several image frames were collected. Ideally, sarcomere images were collected at multiple points within the muscle belly, thus providing a more comprehensive understanding of the sarcomere length of the TA. However, this was not always possible due to patient discomfort or the accumulation of blood clots and other debris on the endoscope probe lens.

To measure sarcomere length from collected images, each frame was first imported into Matlab and rotated such that muscle fibers within each image were oriented vertically. Once this was complete, a one-dimensional Fourier transform was performed along each pixel column for a given frame. For each resulting frequency spectrum, a bandpass filter was used to isolate the range of spatial frequencies which could realistically correspond to the spatial frequency pattern of sarcomeres in the image. The dominant spatial frequency in each filtered spectrum was identified, and the inverse of this frequency value determined the sarcomere length for the given pixel column.

Sarcomere length values were averaged across all pixel columns to generate a sarcomere length measurement for each image frame, and these sarcomere length measurements were averaged across all collected frames for a given subject at a given insertion position to generate a cumulative measure of sarcomere length across all imaged muscle fibers (Figure 3.5) (Chen et al., 2016).

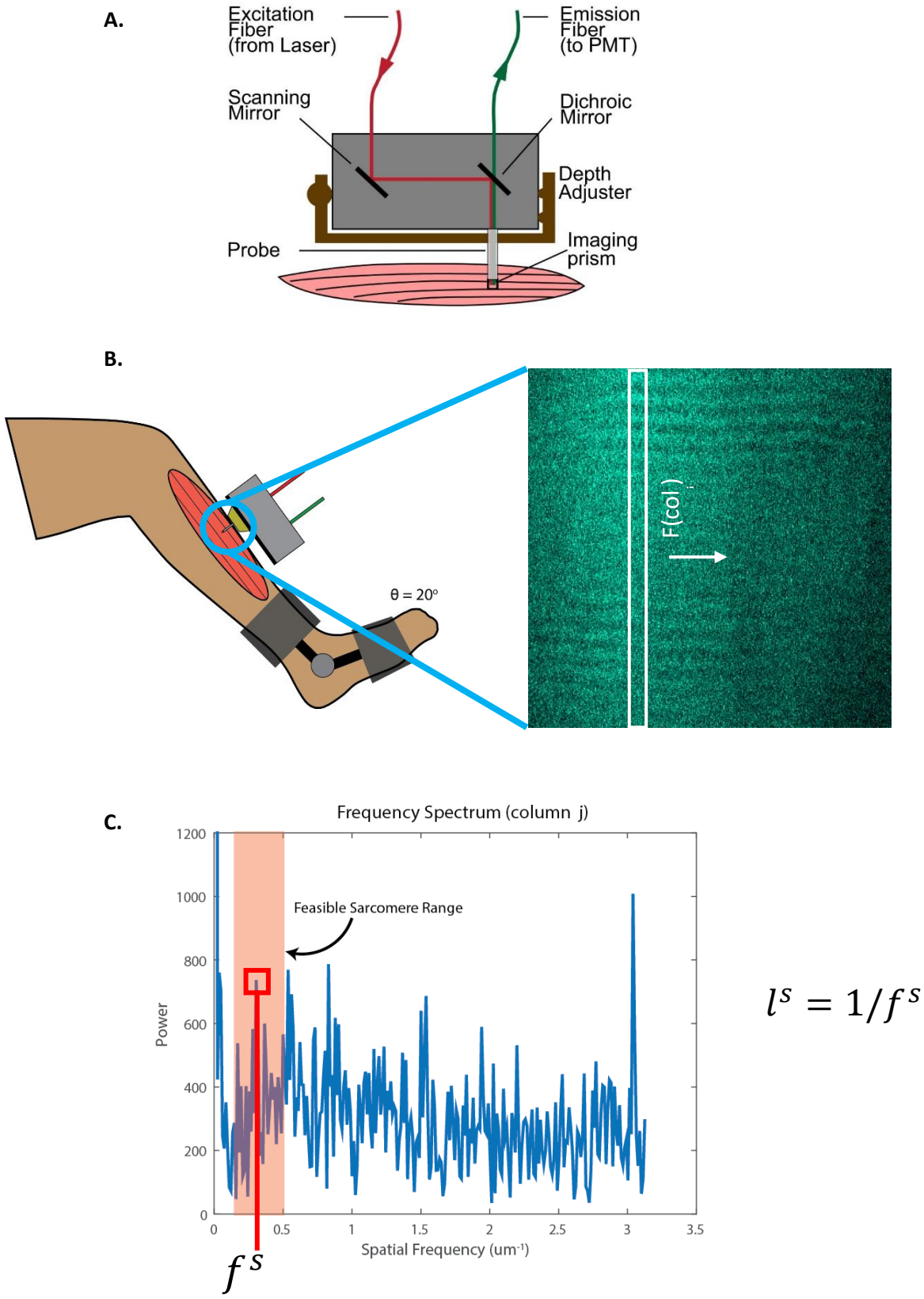

Figure 3.5. ***Measuring Sarcomere Length Using Micro-endoscopic Imaging.*** *(A) The micro-endoscopic imaging system used to image sarcomeres delivered an excitation laser directly to the muscle tissue through an optical needle probe. This generated a second harmonic signal, which was used to develop images of sarcomere arrangement. (B) Images of TA sarcomere structure were collected with the ankle at a joint angle of 20°. (C) Sarcomere length was determined in collected images by performing a 1D Fourier transform on each pixel column. Sarcomere length was calculated as the inverse of the dominant spatial frequency within a feasible sarcomere length range in the resulting frequency spectrum.*

3.5 Dynamometry

To assess torque production capacity of the TA, dynamometric testing was performed using a Biodex dynamometry system (Biodex, Shirley, NY). For each subject, peak isometric torque was measured during maximum voluntary contraction (MVC) of the ankle dorsiflexors following the protocol described in the Biodex user manual. Prior to testing, subjects warmed up by walking at a self-selected speed for approximately 5 minutes within the testing facility. Subjects were then seated and stabilized within the Biodex system. The seatback was set to 80°, and the dynamometer position was adjusted such that the subject's knee on the leg being tested was fixed at a flexion angle of 25°. The subject was stabilized at this position by straps across the abdomen and the thigh of the leg being tested. The axis of the dynamometer was aligned with the anatomical axis of rotation of the ankle joint by visual inspection and palpation, and the foot pedal was adjusted to the appropriate test angle. Four joint angles were tested, beginning with an angle of 10° dorsiflexion and ending with an angle of 20° plantarflexion in increments of 10°. Although isometric testing was performed for both legs, only the results corresponding to the subject's dominant limb are reported in this work. The testing procedure was thoroughly described to each subject, and subjects performed three submaximal voluntary contractions and one MVC prior to testing to gain familiarity with the approach. During testing, three trials of MVC were performed at each joint angle. Contractions were held for 3 seconds, after which, subjects were allowed to rest for 30 seconds. The torque contributions of the dynamometer arm and the weight of the subject's limb were removed prior to subsequent analyses.

To measure peak isometric dorsiflexion torque from the raw voltage data output of each dynamometric test, a fourth order lowpass Butterworth filter was first applied to reduce signal noise. The filtered voltage data was then converted to a torque signal in Nm by applying an

appropriate scaling factor. Further smoothing was performed on this torque signal via a moving average filter with a window size of 1000. The smoothed torque signal was then rectified and shifted such that the initial torque value was 0 Nm. For each test, peak dorsiflexion torque was determined to be the maximum measured torque value within the given signal. For each subject, the reported peak dorsiflexion torque at each joint position is the average of the maximum value across three trials.

3.6 Calculating Physiological and Functional Properties

The measured architectural parameters described above were used to compute the optimal fascicle length (l_{fo}) and PCSA of the TA muscle. l_{fo} was computed by normalizing the measured resting muscle fascicle length at 20° plantarflexion to a sarcomere length of 2.7 μm according to the following equation:

$$l_{fo} = l_f/l_s * 2.7\ \mu m \tag{3.1}$$

where l_f is the fascicle length at 20° measured from ultrasound imaging, 2.7 μm is the assumed optimal sarcomere length for human muscle, and l_s is the measured sarcomere length at 20°. *PCSA* was then calculated according to the following equation:

$$PCSA = V/l_{fo} \tag{3.2}$$

where V is the muscle volume measured from MRI.

The operating range of the TA was then computed by normalizing measured active fascicle lengths by optimum fascicle length and identifying the region of the force-length curve encompassed by the resulting normalized fascicle length values. A theoretical estimate of normalized force production at each joint position of interest for each subject was determined by interpolating the force-length curve at each computed normalized fascicle length.

An estimate of the peak ankle dorsiflexion moment (T_{est}) generated by the TA was then computed from normalized force estimates at each joint position using the following equation:

$$T_{est} = \tilde{F} * R * \cos(\alpha) \quad (3.3)$$

where $\tilde{F}$ is the estimated normalized active force production of the TA, R is the TA moment arm, and α is the muscle pennation angle. Because this torque estimate is the product of a theoretical normalized force and several measured quantities, its true value is meaningless. Thus, torque estimates were normalized by their maximum value across joint positions for each subject.

To compare theoretical estimates of TA dorsiflexion torque capacity with measured torques, the contribution of the TA to total measured dorsiflexion torque was first isolated. Peak isometric moment curves were generated for each ankle dorsiflexor muscle in the OpenSim biomechanics software platform (SimTK, Mountain View, CA) using the Gait2392 lower limb model (Thelen et al., 2012). At each joint position of interest in this study, the ratio of TA dorsiflexion moment to total dorsiflexion moment was determined and used to scale the total measured dorsiflexion moment from dynamometry. Isolated TA dorsiflexion moments were then normalized to their maximum value across joint positions for each subject.

3.7 Error Analysis and Statistics

Architecture-based estimates of TA torque capacity and measured torque values were plotted against joint position and compared through visual inspection of trends and ranges of each curve. Discrepancies between estimated and measured values were then quantified by computing the RMS differences between the two curves. The sensitivity of our torque estimation approach to methodological choices and changes in the values of measured parameters was then evaluated.

Three methodological factors were identified as having the potential to influence the results of our torque estimation procedure: (1) the decision to fit a second order polynomial to tendon excursion data rather than a higher order polynomial during moment arm estimation; (2) the assumption that optimal sarcomere length in humans is 2.7 µm (Woledge et al., 1985), rather than the 2.8 µm optimal sarcomere length value reported by Walker and Schrodt (1974); and (3) the decision not to scale measured sarcomere lengths from micro-endoscopy to account for deformation of muscle fibers around the imaging probe, as described by (Chen et al., 2016). For each of the above considerations, there exists published literature supporting our original methodological choices, as well as the alternative approaches. Thus, it was desirable to explore the roles these three factors play on torque estimation from architectural measurements (Table 3.2).

Methodological Variants	Original	Alternative
Tendon Excursion Data Fitting for Moment Arm Calculation	2nd Order Polynomial	3rd Order Polynomial (MA3)
Assumed Optimal Sarcomere Length	2.7 µm	2.8 µm (LS2.8)
Accounting for Sarcomere Deformation Around Endoscope Probe	None	Scale by 0.91 (DC)

Table 3.2. ***Sensitivity of Torque Estimates to Methodological Variants.*** *The table above shows the three methodological variants being considered for their potential impact on TA torque estimates, including the original method choice and the alternatives supported by the literature.*

Estimated TA torque capacity was recalculated for all subjects using each methodological variant and keeping all other parameter values constant. In the case of the method used to compute moment arm, a third order polynomial was fit to tendon displacement versus joint position data rather than the original second order polynomial. As before, this curve was differentiated to

estimate moment arm via the tendon excursion method. Torque estimates were then computed using these alternative moment arm values. Similarly, the impact of human optimal sarcomere length on estimated torque was determined by recalculating torque using 2.8 μm when computing optimal fascicle length rather than the original assumed value of 2.7 μm. Lastly, the influence of correcting sarcomere lengths to account for fiber deformation around endoscopic probes during imaging was evaluated by scaling measured sarcomere lengths by a factor of 0.91 and re-computing torque as before. A scaling factor of 0.91 was selected based on Chen et al. (2016) who reported that sarcomere lengths far from micro-endoscopic probes were 91% shorter than those in close proximity to the probe, indicating that sarcomeres measured during micro-endoscopic imaging are likely longer due to deformation around the probe. As before, all torque estimates were normalized to their maximum value across joint angles for each subject.

A two-factor repeated measures ANOVA with Tukey-Kramer post-hoc testing was performed to identify effects of estimation method (factor 1) and joint angle (factor 2) on dorsiflexion torque estimates. Measured dorsiflexion torque data was also included in this ANOVA to determine if significant differences exist between measured joint torque and the various estimation procedures. To identify specific effects at each joint position, two-tailed paired-sample T-tests were performed between each estimate method (including dynamometric measurement) pair.

A sensitivity analysis was performed to evaluate the effect of each measured architectural parameter on estimated joint torque. For each measured architecture parameter of the TA (fascicle length, pennation angle, moment arm, and sarcomere length), the estimated joint torque was recalculated twice with the parameter value either raised or lowered by one within-subject measurement standard deviation. Again, all torque estimates were normalized to their maximum

value across joint positions for each subject. The sensitivity of the torque estimate to each parameter was quantified by calculating the root mean squared difference between the -1 SD torque curve and the +1 SD torque curve.

To determine the cumulative effect that methodological variants and parameter sensitivity have on architecture-based estimates of muscle torque production, a final torque calculation was carried out in which methodological variants were selected and architectural parameters were lowered or raised by one standard deviation in order to maximize or minimize the resulting torque estimate for each subject. These torque estimates were again normalized, providing an indication of the maximum feasible range of estimated torque values that can be expected from an architecture-based muscle torque estimation procedure.

4 Results

This chapter presents the results of our experimental data collection, including the values of measured architectural and functional properties of the tibialis anterior. The first estimates of optimal fascicle length and PCSA derived entirely from *in vivo* architecture measurements are then reported. The operating length range and estimated torque production capacity of the TA are described, and the sensitivity of estimated torque to methodological decisions and measured parameter values is discussed. Note that measured properties are reported as the mean and standard deviation across subjects unless states otherwise. A summary of measured TA architecture data is presented in Table 4.1.

Subject	Muscle Volume (cm^3)	Resting Fascicle Length (cm)				Active Fascicle Length (cm)				Resting Pennation Angle (°)				Active Pennation Angle (°)				Moment Arm (cm)				Sarcomere Length (μm)	Optimal Fascicle Length (cm)	PCSA (cm^2)
		Joint Angle				Joint Angle				Joint Angle				Joint Angle				Joint Angle						
		-10	0	10	20	-10	0	10	20	-10	0	10	20	-10	0	10	20	-10	0	10	20			
Subject 1	149	5.1	5.4	5.8	6.3	4.6	5.1	5.6	6.2	12.8	11.8	9.4	8.8	13.2	11.7	10.7	10.1	4.2	4.0	3.7	3.4	2.89	5.90	25.3
Subject 2	119	5.1	5.8	6.5	6.7	4.7	4.9	5.5	5.7	10.7	10.2	7.7	7.8	12.8	11.7	10.8	9.5	1.7	1.7	1.7	1.8	2.68	6.79	17.5
Subject 3	184	4.8	5.9	6.5	6.6	4.7	5.6	6.4	6.6	13.4	11.7	11.0	8.7	14.0	12.6	10.2	10.0	3.6	3.3	3.1	2.8	2.77	6.44	28.6
Subject 4	264	6.1	6.9	7.4	8.2	5.1	5.6	6.3	7.0	13.2	11.2	9.9	9.2	15.4	13.3	12.1	10.4	3.8	3.8	3.7	3.7	2.68	8.29	31.8
Subject 5	136	6.4	7.0	7.3	7.6	5.0	5.7	6.1	6.5	10.7	9.1	7.8	7.3	12.6	11.6	9.5	9.2	6.7	6.1	5.5	5.0	2.68	7.69	17.7
Mean (S.D.)	170.4 (57.5)	5.5 (0.8)	6.2 (0.8)	6.6 (0.8)	6.9 (0.9)	4.8 (0.7)	5.4 (0.5)	6.0 (0.7)	6.5 (0.8)	12.1 (2.2)	10.8 (2.0)	9.2 (1.9)	8.3 (1.4)	13.6 (1.8)	12.2 (1.4)	10.6 (1.3)	9.9 (1.3)	4.2 (1.9)	3.9 (1.6)	3.7 (1.4)	3.4 (1.2)	2.74 (0.09)	7.02 (0.96)	24.2 (6.44)

Table 4.1. ***Summary of TA Architecture Measurements.*** *The above table summarizes collected muscle architecture data for all subjects and provides and average and standard deviation of architecture measurements across subjects.*

4.1 Tibialis Anterior Architecture and Measured Functional Capacity

The average volume of the TA across subjects was 170.4 ± 57.5 cm^3. This value is more than twice as large as the volume reported previously in a comprehensive cadaver dissection study (Ward et al., 2009) of 75.6 ± 25.1 cm^3, but is in agreement with the TA volume of 135.2 ± 27.5 cm^3 reported by Handsfield et al. in their 2014 MRI study (Figure 4.1).

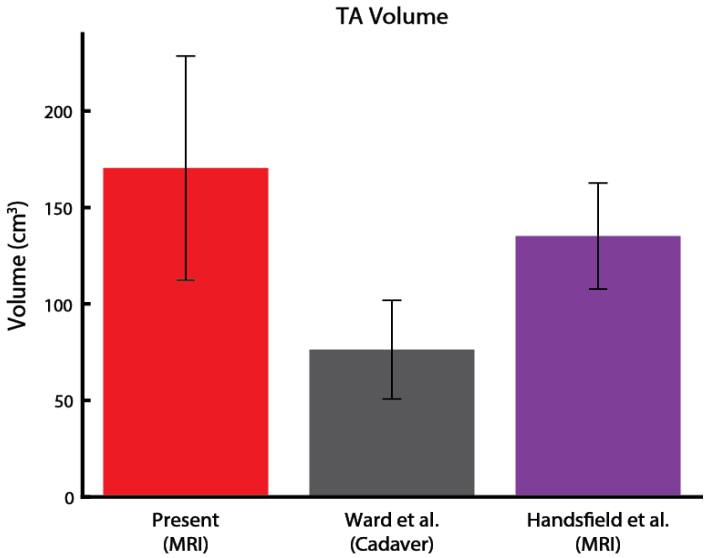

Figure 4.1. ***Measured TA Volume and Comparison to Published Data.*** *Average TA volume measured using MRI compared to published data by Ward et al. (2009) and Handsfield et al. (2014).*

As expected, measured fascicle lengths increased with increasing ankle plantarflexion. Fascicle lengths were also consistently higher in the resting state than in the active state for corresponding ankle joint positions, demonstrating an average shortening of 0.63 cm. In the resting state, measured fascicle lengths ranged from 4.8 to 8.2 cm for individual subjects, with average values across subjects of 5.5 ± 0.8 cm, 6.2 ± 0.8 cm, 6.6 ± 0.8 cm, and 6.9 ± 0.9 cm at joint angles of -10°, 0°, 10°, and 20°, respectively. For the same joint angles in the active state, average fascicle lengths were measured at 4.8 ± 0.7 cm, 5.4 ± 0.5 cm, 6.0 ± 0.7 cm, and 6.5 ± 0.8 cm with values ranging from 4.6 to 7.0 cm for individual subjects. Within-subject standard deviations were

consistently around 10% of measured values, with average repeated-measure standard deviations across subjects and joint angles of 0.6 cm (resting) and 0.6 cm (active). The values reported here are smaller than those measured by Maganaris and Baltzopoulos (1999) in their ultrasound-based architecture study for the TA at rest, but agree well with published data for the TA in the maximally active state. Specifically, Maganaris and Baltzopoulos measured average fascicle lengths ranging from ~7 to ~9 cm at joint angles from 15° dorsiflexion to 30° plantarflexion when the TA is at rest and lengths ranging from ~4 to ~6 cm when the muscle is maximally activated. Because active state architecture was used in the present study to estimate functional capacity, this agreement supports the accuracy of our methods (Figure 4.2).

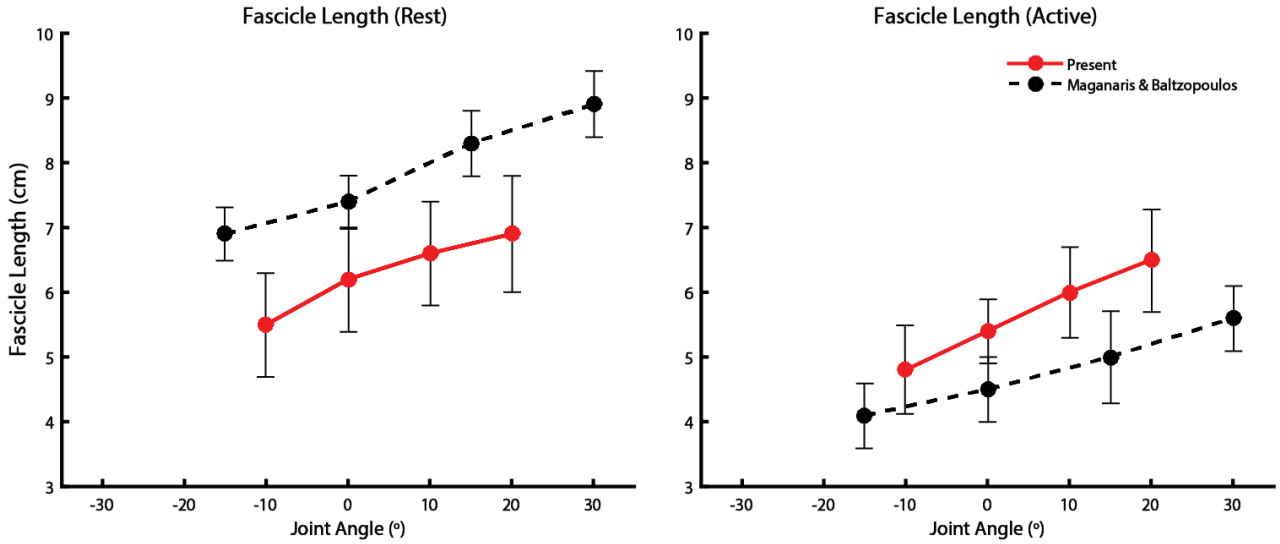

Figure 4.2. ***Resting and Active TA Fascicle Length and Comparison to Published Data.*** *Average TA fascicle length was measured in both the resting (left) and maximally active (right) states at four ankle joint positions. Results are compared to published data by Maganaris and Baltzopoulos (1999).*

TA pennation angle decreased with increasing ankle plantarflexion and was consistently higher in the active state than in the resting state for corresponding ankle joint positions. In the resting state, pennation angle was measured at 12.1 ± 2.2°, 10.8 ± 2.0°, 9.2 ± 1.9°, and 8.3 ± 1.4° at joint angles of -10°, 0°, 10°, and 20°, respectively. For the same joint angles in the active state,

pennation angle was measured at 13.6 ± 1.8°, 12.2 ± 1.4°, 10.6 ± 1.3°, and 9.9 ± 1.2°. Again, within-subject standard deviations were consistently around 10% of measured values, with average repeated-measure standard deviations across subjects and joint angles of 1.5° (resting) and 1.3° (active). Measured values agree well with those reported by Maganaris and Baltzopoulos (1999) for resting state architecture, but are smaller than the pennation angles reported for maximally contracted muscle in that work. The authors measured pennation angle to range from ~13° at -15° dorsiflexion to ~9° at 30° plantarflexion for the TA in the resting state, and from ~22° to ~16° for the TA in the maximally active state (Figure 4.3). The large increase in TA pennation angle between the resting and active states reported by Maganaris and Baltzopoulos, in addition to the large decrease in fascicle length relative to our findings, indicate that a greater amount of muscle shortening occurred during maximum voluntary contraction in the Maganaris and Baltzopoulos study than in our own. The authors do not indicate if/how ankle position was maintained during contraction in their work, but it may be that non-isometric muscle contraction gave rise to the discrepancies in these measurements observed here.

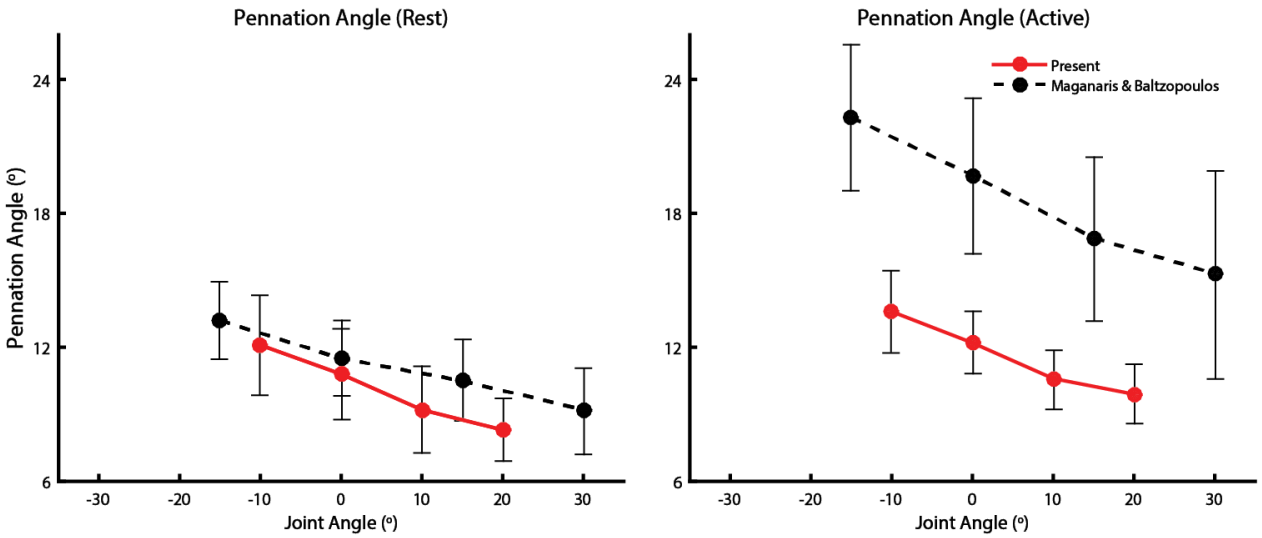

Figure 4.3. ***Resting and Active TA Pennation Angle and Comparison to Published Data.*** *Average TA pennation angle was measured in both the resting (left) and maximally active (right) states at four ankle joint positions. Results are compared to published data by Maganaris and Baltzopoulos (1999).*

In agreement with previously published moment arm data, the measured moment arm of the TA, on average, decreased with increasing ankle plantarflexion. This trend held true at the individual subject level as well, with the exception of subject 2, who showed a slight increase in TA moment arm with increased plantarflexion. Across subjects, measured moment arm ranged from 1.7 to 6.7 cm, with average values of 4.2 ± 1.9 cm, 3.9 ± 1.6 cm, 3.7 ± 1.4 cm, and 3.4 ± 1.2 cm at joint angles of -10°, 0°, 10°, and 20°, respectively. Within-subject standard deviations were higher for moment arm measurements than for other ultrasound-based measurements, with an average repeated-measure standard deviation across subjects and joint angles of 0.9 cm.

The results reported here are in agreement with published TA moment arm data from some previous tendon excursion studies, but deviate from others. Maganaris (2000) used the tendon excursion method to measure TA moment arm in both the resting and maximally contracted state, finding that moment arm ranged from ~5.5 cm to ~3 cm across the ankle range of motion (30° dorsiflexion to 30°) regardless of the muscle activation state. These results are similar to those reported in our work. In contrast, Ito et al. (2000) used tendon excursion to measure TA moment arm at several levels of muscle activation, finding that moment arm ranged from ~2.5 cm to ~1.5 cm at rest and from ~4.5 cm to ~3 cm at all activation levels greater than 30% maximal. These results are comparable to those reported above for muscle in the active state but deviate in the resting state, despite our measurements taking place with the muscle at rest (Figure 4.4).

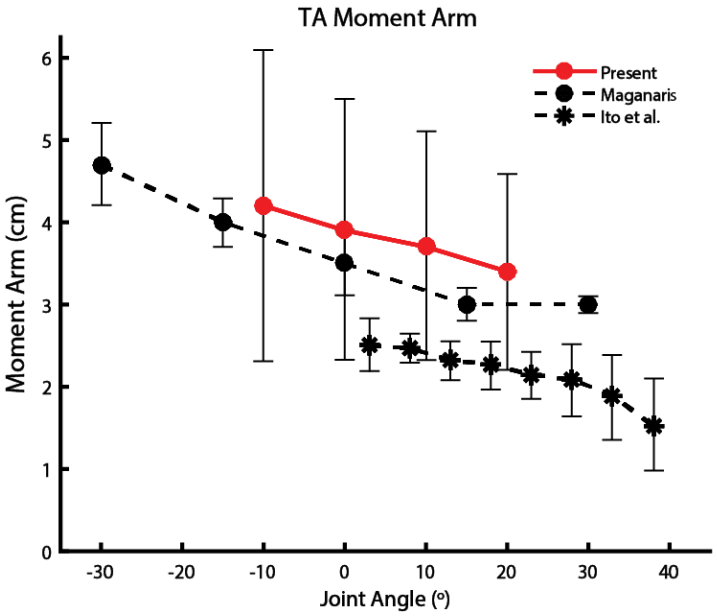

Figure 4.4. ***TA Moment Arm and Comparison to Published Data.*** *Average moment arm of the TA was measured at four ankle joint positions. Results are compared to published data by Maganaris et al. (2000) and Ito et al. (2000).*

Sarcomere length was measured at 2.74 ± 0.09 µm at an ankle joint angle of 20° plantarflexion, indicating that the sarcomeres of the TA are operating near their optimal length of 2.7 µm when the TA is plantarflexed. Within-subject standard deviations for sarcomere measurements were as high as 21%, with an average repeated-measure standard deviation across subjects of 0.38 µm. To our knowledge, *in vivo* measurements of sarcomere length in the human TA have not been reported previously. The sarcomere length reported here is smaller than that reported by Ward et al. (2009) in their cadaver dissection study; however, because the positioning of the ankle during measurement is not described by Ward et al., and because the effects of death and fixation processes on sarcomere structure and arrangement are not fully known, this comparison is not indicative of a problem with our data (Figure 4.5).

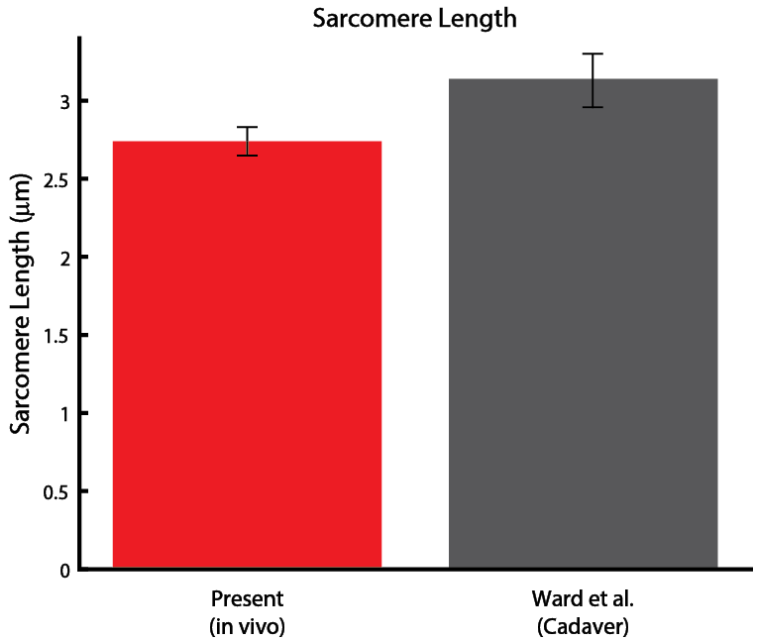

Figure 4.5. ***Average TA Sarcomere Length and Comparison to Published Data.*** *Average TA sarcomere length was measured at an ankle joint angle of 20° plantarflexion. Results are compared to published data by Ward et al. (2009).*

Average peak isometric dorsiflexion torque across subjects was measured to be 20.0 ± 7.6 Nm, 29.7 ± 14.7 Nm, 35.4 ± 14.9 Nm, and 40.8 ± 16.9 Nm at joint angles of -10°, 0°, 10°, and 20°, respectively. These measurements were found to be highly repeatable, with an average repeated measure standard deviation across subjects and joint angles of 2.2 Nm. The values reported here are in good agreement with previously published dynamometric measures of peak isometric dorsiflexion torque (Geboers et al., 2000). Using OpenSim software, it was found that the contribution of the TA to total dorsiflexion torque is 54.52%, 54.84%, 54.89%, and 54.65% at joint angles of -10°, 0°, 10°, and 20°, respectively. Measured peak dorsiflexion torque values were scaled by these percentages, revealing the isolated contribution of the TA to peak torque to be 10.9 ± 1.2 Nm, 16.3 ± 0.7 Nm, 19.4 ± 1.5 Nm, and 22.3 ± 1.1 Nm (Figure 4.6).

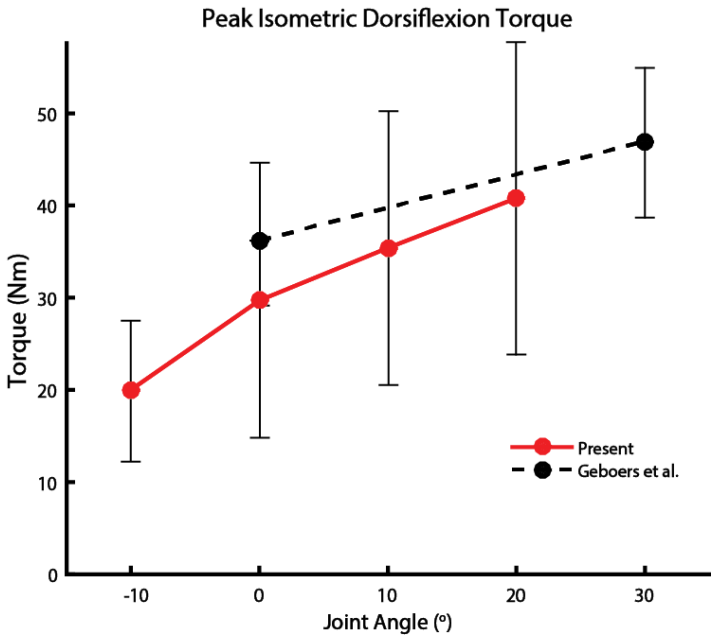

Figure 4.6. ***Average Peak Dorsiflexion Torque and Comparison to Published Data.*** *Average peak dorsiflexion torque was measured at four ankle joint positions. Results are compared to published data by Geboers et al. (2000).*

4.2 Optimal Fascicle Length and PCSA

Using the above architectural parameters, the optimal fascicle length of the TA was calculated to be 7.02 ± 0.69 cm. This measure of optimal fascicle length is in close agreement with the value of 6.83 ± 0.79 reported in Ward et al. (2009). The PCSA of the TA was calculated to be 24.17 ± 6.43 cm^2. This measure of PCSA is larger than that reported in Ward et al., likely due to the large difference in measured muscle volumes between their cadaver-based study and our *in vivo* study. Fukunaga et al. (1992) used a hybrid approach to estimate the PCSA of the TA, measuring TA volume using MRI, but using a cadaver-derived estimate of optimal fascicle length to compute PCSA. The value of PCSA reported by Fukunaga et al. is in agreement with that reported here. To our knowledge, these are the first measures of human optimal fascicle length and PCSA derived entirely from *in vivo* measurements (Figure 4.7).

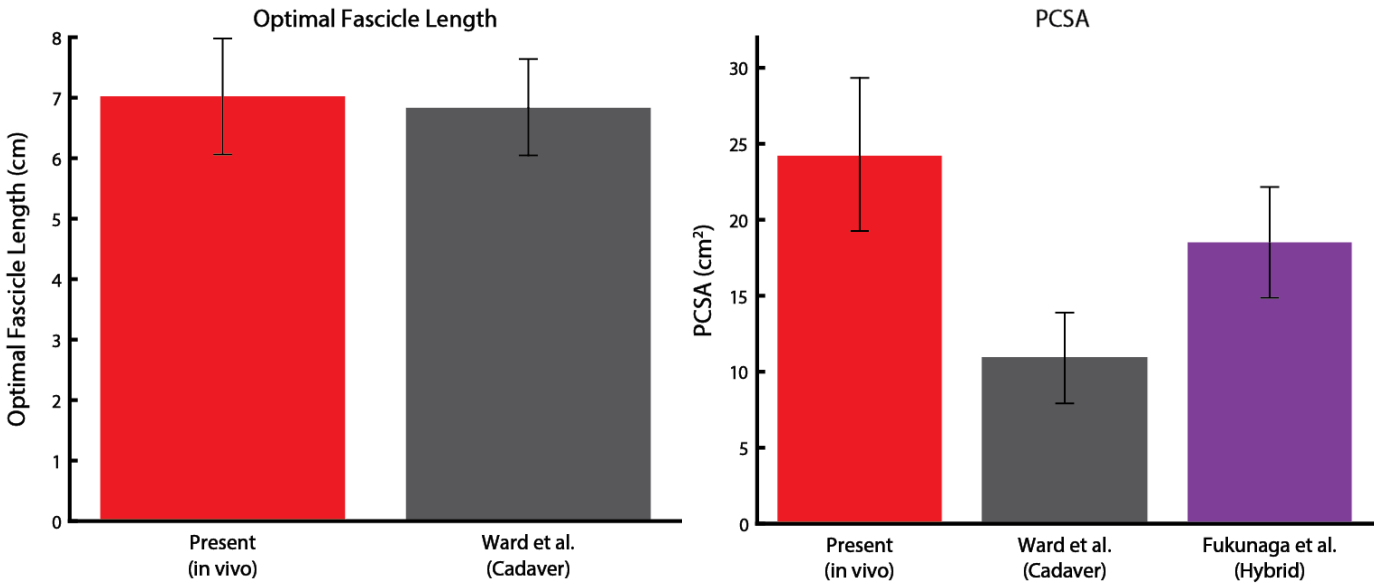

Figure 4.7. ***Optimal Fascicle Length and PCSA of the TA.*** *Average optimal fascicle length of the TA is reported and compared to data published by Ward et al. (2009). Average PCSA of the TA is compared to data published by Ward et al. (2009) and Fukunaga et al. (1992).*

4.3 Tibialis Anterior Operating Range

Normalizing measured active TA fascicle lengths by optimal fascicle length revealed that, across subjects, the TA tended to operate on the upper ascending limb and plateau regions of the muscle active length-tension curve (Figure 4.8). Normalized fascicle lengths ranged from 0.62 to 1.06 with average values of 0.69 ± 0.06, 0.77 ± 0.08, 0.86 ± 0.10, and 0.92 ± 0.11 at joint angles of -10°, 0°, 10°, and 20°, respectively (Table 4.2). These normalized fascicle lengths correspond to a normalized force production capacity of 0.71 ± 0.14, 0.84 ± 0.08, 0.92 ± 0.07, and 0.94 ± 0.05, respectively. Because measured ankle dorsiflexion torque approximately doubled while TA tendon moment arm tended to decrease across the range of joint positions being considered in this study, it was expected that the TA operates largely on the ascending limb of the force length curve, as this would allow the muscle to produce steadily more force as ankle plantarflexion increases, thus enabling greater torque production. However, the fact that estimates of TA operating range based on architecture measurements are clustered around the plateau provided the first indication of a

discrepancy between measured muscle function and architecture-derived estimates of muscle function.

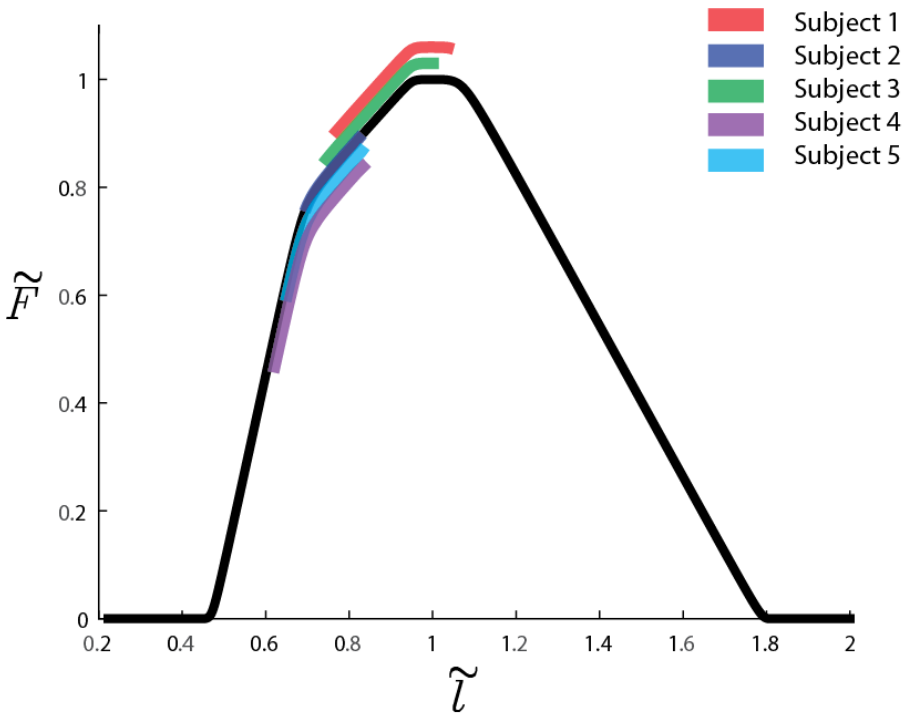

Figure 4.8. ***Operating Range of the TA.*** *The operating length range of the TA was determined by normalizing measured fascicle lengths at each joint position of interest by optimal fascicle length. The region of the length-tension curve over which the TA of each subject operates was then determined.*

Subject	-10°	0°	10°	20°
1	0.767	0.863	0.942	1.058
2	0.690	0.716	0.811	0.840
3	0.736	0.866	0.997	1.017
4	0.616	0.690	0.761	0.842
5	0.655	0.739	0.799	0.845
Mean	0.693	0.775	0.862	0.920

Table 4.2. ***Normalized Lengths of the TA Across Ankle Range of Motion***

4.4 Comparing Theoretical and Measured Torque

An estimate of normalized peak dorsiflexion torque was computed for each subject by multiplying theoretical normalized force production described above by measured moment arm and cosine of pennation angle, and then normalizing results to their maximum value for a given subject. Visual comparison between estimated and measured normalized torque curves indicated that the range of values encompassed and the curve shape were the two primary factors distinguishing the two curve types, although the magnitude of these differences varied considerably across subjects. The range of each torque curve was quantified by simply subtracting the minimum value from the maximum value (Figure 4.9). A one-tailed paired-sample T-test determined that the range of the measured dorsiflexion torque curves was significantly higher than the range of the estimated torque curves ($p = 0.0012$). Differences in curve shape were quantified by calculating the root mean squared (RMS) difference between the measured and estimated torque curves. Across subjects, the RMS difference ranged from 0.20 to 0.60, with an average value of 0.41, which is quite large relative to the scale of the two curves (Table 4.3).

A two-factor ANOVA revealed that both ankle joint position and the method of estimation/measurement had a significant effect on dorsiflexion torque ($p = 0.0014$ and $p = 8.227 \times 10^{-4}$, respectively), although a significant interaction does exist between the two factors ($p = 4.348 \times 10^{-6}$). Post-hoc testing found that torque data generated via the original architecture-based estimation approach were significantly different from torque data measured via dynamometry ($p = 0.0002$). Two-tailed paired-sample T-tests performed at each joint angle of interest revealed that the effect between estimated dorsiflexion torque and measured dorsiflexion torque was significant at 10° dorsiflexion ($p = 0.0014$) (Figure 4.10).

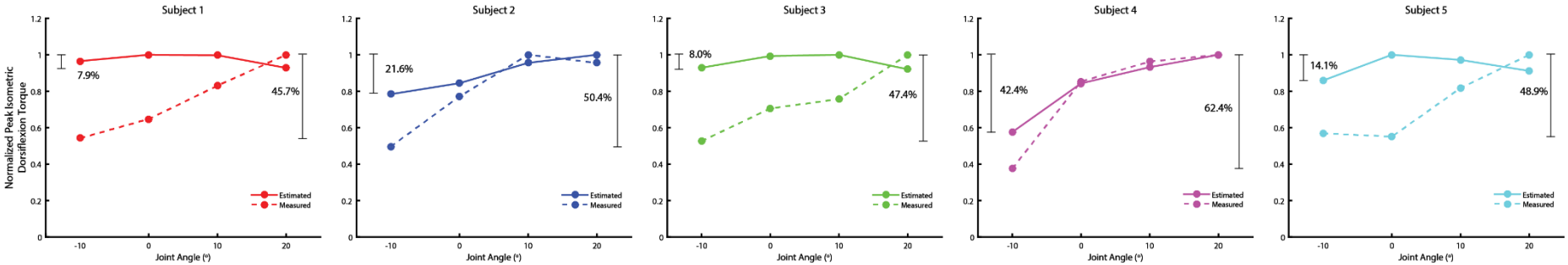

Figure 4.9. ***Comparison Between Architecture-Based Estimates of TA Torque Capacity and Measured TA Torque Capacity.*** *Normalized TA torque capacity was computed at each ankle joint position using architecture mesaurements and compared to dynamometry measurements of peak dorsiflexion torque. The range of total torque capacity covered by each curve, expressed as a percentage, is indicated.*

Subject	RMS Difference
1	0.601
2	0.220
3	0.557
4	0.202
5	0.549
Average	0.413

Table 4.3. ***Root Mean Squared Differences Between Architecture-Based Torque Capacity Estimates and Measured Torque***

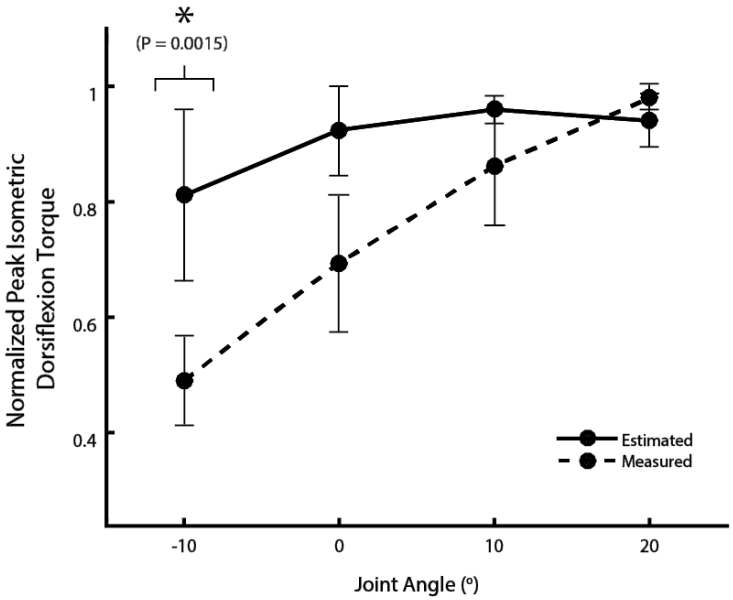

Figure 4.10. ***Comparison Between Average Estimated TA Torque Capacity and Average Measured Torque Capacity.*** *Average estimated and measured torque curves are significantly different at a joint position of -10° (paired sample T-test, $p < 0.005$)*

4.5 Influence of Methodological Choices on Torque Estimate

Calculating estimated torque using the aforementioned methodological variants was found to have no significant effect on estimated torque values, according to the results of a two-factor ANOVA and post-hoc analysis (Table 4.4, 4.5). Torque estimates computed using the three methodological variants were not significantly different from the original estimate of dorsiflexion torque, and were all significantly different from measured dorsiflexion torque ($p < 0.05$). This result was confirmed through two-tailed paired-sample T-tests performed between each pair of torque estimation methods at each ankle joint position of interest, with the exception of scaling measured sarcomere lengths to account for fiber deformation around the endoscopic probe, which was found to be significantly different than the original torque estimate only at a joint position of 10° dorsiflexion (Figure 4.11). These results indicate that the methodological variants considered in this work have minimal impact on torque estimation, although their cumulative effect could be significant.

Factor	P-value
Joint Position	*0.0014
Estimation Method	*8.2274×10^{-4}
Position x Method	*4.348×10^{-6}

Table 4.4. ***Methodological Variant 2-Way ANOVA Results.*** *(* denotes statistical significance, $p < 0.05$)*

Estimation Method	-10°	0°	10°	20°
Original x MA3	0.6990	0.2759	0.4620	0.7251
Original x LS2.8	0.0561	0.1785	0.4416	0.2631
Original x DC	*0.0186	0.0925	0.9172	0.1459
Original x Measured	*0.0015	0.0557	0.1629	0.2103
MA3 x LS2.8	0.1218	0.5021	0.4168	0.5973
MA3 x DC	*0.0199	0.1728	0.4165	0.4130
MA3 x Measured	*0.0027	0.0652	0.2373	0.2705
LS2.8 x DC	*0.0087	0.0753	0.7684	0.1035
LS2.8 x Measured	*0.0092	0.1192	0.1626	0.2705
DC x Measured	0.0796	0.2951	0.1938	0.4913

Table 4.5. ***Methodological Variant Paired-Sample T-test Results.*** *Paired-sample T-tests were performed between data of each methodological variant pair at each joint position. (* denotes statistical significance, $p < 0.05$)*

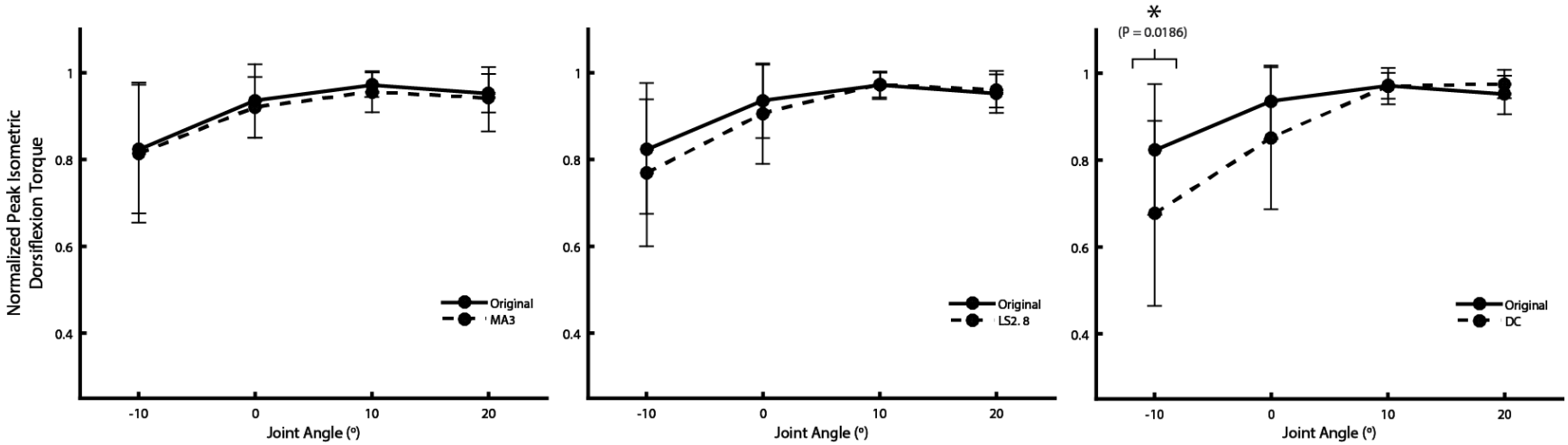

Figure 4.11. ***Effects of Methodological Variants on Estimated Torque Results.*** *TA torque capacity was estimated at each joint position for each methodological variant and compared with original torque estimates. (* denotes statistical significance, paired-sample T-test, $p < 0.05$)*

4.6 Sensitivity of Torque Estimate to Measured Parameters

The sensitivity of estimated torque to the values of the four measured parameters (moment arm, fascicle length, pennation angle, and sarcomere length) was evaluated by altering the values of each parameter individually by one standard deviation and observing the change in estimated torque values. Estimated torque was found to be moderately sensitive to the value of moment arm and fascicle length. The impact of altering these parameters was more pronounced at lower joint angles (-10° dorsiflexion and neutral) and minimal at 10° plantarflexion. Estimated torque was not sensitive to pennation angle, as altering its value had little effect on the resulting torque values. In contrast, estimated torque was found to be most sensitive to measurements of sarcomere length. Altering the value of sarcomere length resulted in a wide range of torque estimates about the original estimate. As with other parameters, this range was widest at lower joint angles (-10° dorsiflexion and neutral) and smallest at 10° plantarflexion (Figure 4.12). Parameter sensitivity was quantified by computing the root mean squared difference between the torque estimate calculated using the +1 SD parameter value and the estimate calculated using the -1 SD parameter value for each subject. The average RMS difference across subjects was smallest for pennation angle at 0.004, moderate for moment arm and fascicle length at 0.167 and 0.141, respectively, and largest for sarcomere length at 0.383 (Table 4.6).

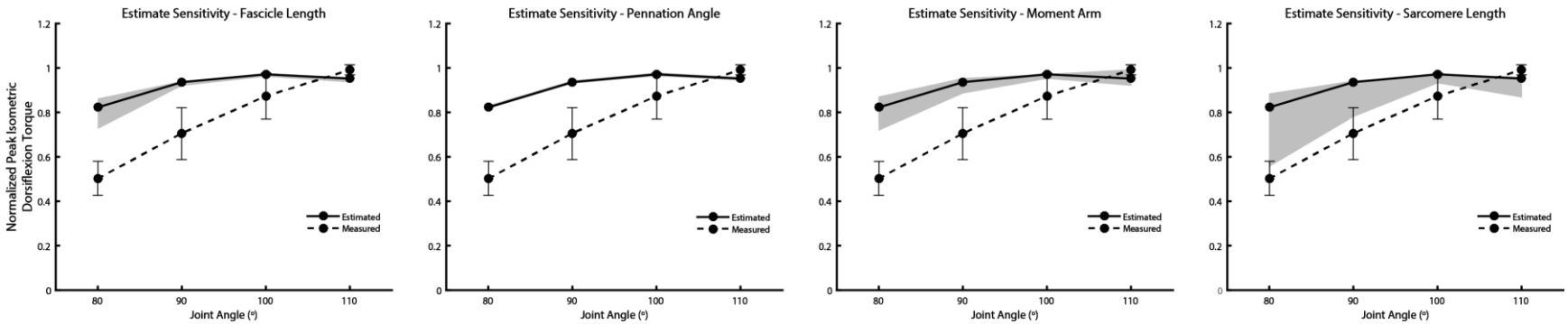

Figure 4.12. ***Sensitivity of Torque Estimates to Architecture Parameter Values****. TA torque capacity was calculated while varying one architectural parameter value by +/- 1 standard deviation. The gray area denotes the region bounded by the +1 S.D. and -1 S.D. torque estimate curves.*

Subject	Fascicle Length	Pennation Angle	Moment Arm	Sarcomere Length
1	0.108	0.005	0.072	0.519
2	0.427	0.004	0.341	0.649
3	0.356	0.009	0.064	0.117
4	0.085	0.009	0.212	0.181
5	0.104	0.004	0.081	0.671
Average Torque Curve	0.167	0.004	0.141	0.383

Table 4.6. ***Sensitivity of Torque Estimates to Architecture Parameter Values, Quantified by Root Mean Squares.*** *The root mean squared (RMS) difference between the lower bound (-1 S.D.) and upper bound (+1 S.D.) torque estimate curves was computed for each subject for each architectural parameter being altered, providing an measure of the size of the region containing a feasible estimate of TA torque. A larger RMS value indicates that the associated architecture parameter has a larger effect on estimated torque.*

To evaluate the cumulative impact of all methodological choices and parameter sensitivities on estimated torque, dorsiflexion torque was recalculated for each subject with methodological variants selected and parameter values altered by one standard deviation to minimize or maximize the resulting torque estimate. This yielded two torque curves, which form the theoretical upper and lower bound of feasible torque estimates for each subject. The results of these calculations were extreme, generating a large bounded region of feasible torque estimates for each subject. The bounded region was largest at smaller ankle joint angles and tended to decrease with increased plantarflexion. For nearly all subjects, this torque sensitivity region fully encompassed the measured dorsiflexion torque curve for at least three ankle joint positions (Figure 4.13). These results indicate that, while methodological variants had minimal effect on torque estimates and sensitivity of torque estimates to measured parameters was insufficient to explain discrepancies between estimated and measured values, the cumulative effect of methodological choices and measurement variability is sufficient to alter estimated torques in such a way that they more closely agree with measured values.

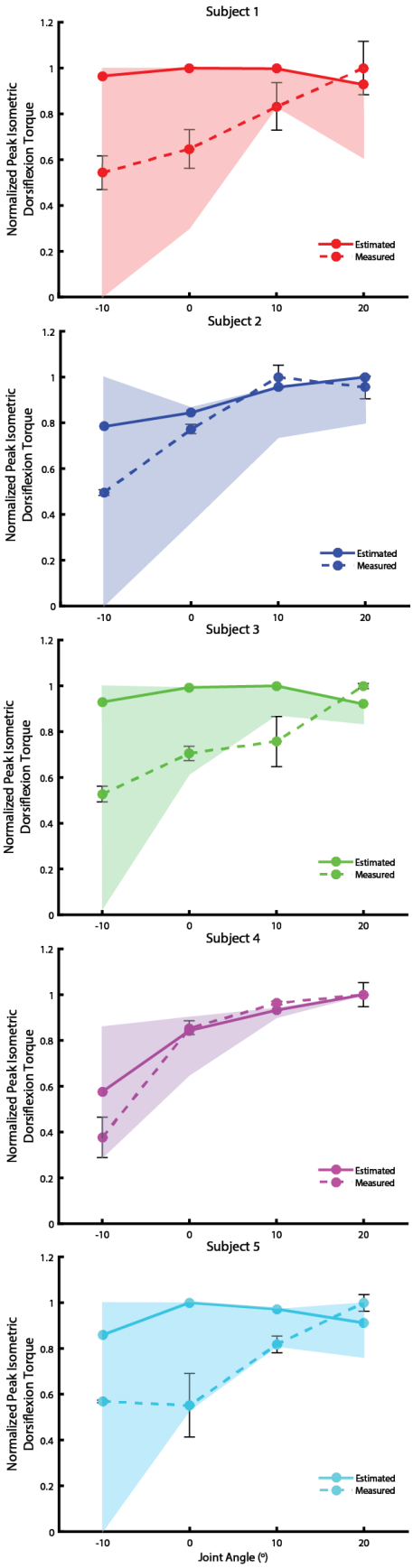

Figure 4.13. ***Cumulative Effect of Methodological Variants and Architecture Sensitivity on Torque Estimtes.*** *For each subject, a lower and upper bound on estimated torque were generated by selectively using methodological variants and altering architecture parameter values +/- 1 S.D. to minimize or maximize the resulting torque estimate. The region contained by these bounding estimate curves is shown for each subject and provides an indication of the cumulative sensitivity of muscle torque estimates to methodology and measurement error.*

5 Discussion

The goals of this study were to (1) generate comprehensive architecture data for the tibialis anterior muscle using *in vivo* techniques, (2) derive an estimate of muscle functional capacity using a theoretical framework and compare this estimate to measured functional capabilities, and (3) evaluate the influence of experimental and methodological considerations on architecture-based estimates of muscle function. The discussion herein provides an explanation of our results, describes the significance of several assumptions and limitations of our methods, and proposes future directions for improving muscle architecture data collection and the modeling techniques that make use of this information.

5.1 Summary and Implications

The findings from this work reveal that: (i) architecture measurements generated through *in vivo* imaging differ from those generated through cadaver dissection, but inconsistently agree with architecture data reported from similar *in vivo* studies; (ii) architecture-based estimates of TA functional capacity do not accurately represent measured functional behavior, and (iii) estimates of muscle function derived from architecture are most sensitive to measurements of sarcomere length, while sensitivity to other parameters and methodological changes is low. Despite this low sensitivity, the cumulative effects of all sources of variability are sufficient to explain differences between estimated and measured joint torques.

The most comprehensive cadaver dissection study of lower limb muscle architecture was performed by Ward et al. (2009), while many pieces of *in vivo* architecture data have been collected across many disparate studies. Both muscle volume and sarcomere length measurements presented in this study are more than one standard deviation different from those reported by Ward et al. The

average TA volume of 170.4 cm^3 reported here is much larger than that reported in Ward et al. This discrepancy is believed to be due to age related muscle loss in the cadaver specimens, whose average was 83 years compared to the 33.6 years of our healthy subjects. The PCSA reported by Ward et al. was also smaller than that measured here, but that difference is explained by the difference in muscle volume, which is used to compute PCSA. Average *in vivo* sarcomere length was considerably smaller than that measured by Ward et al. at 2.74 μm compared to 3.14 μm. The reason for this difference is unclear, but it is likely the result of methodological challenges associated with cadaveric muscle studies, including deformation of tissue samples that are removed from their physiological position. The ankle joint angle at which cadaver specimens were fixed is not reported by Ward et al., so it is also possible that specimen ankles were fixed in a more plantarflexed position, thus giving rise to relatively large sarcomere length measurements. However, the fact that optimal fascicle length is comparable between our study and that of Ward et al. indicates that sarcomere stretching during cadaveric measurements was the likely source of error.

The architecture results reported here are inconsistent in their agreement with other *in vivo* measurements, although ours is the first work to measure *in vivo* architecture comprehensively in the same subjects. For example, comparison with TA fascicle length measurements made by Maganaris and Baltzopoulos (1999) using *in vivo* ultrasound found that our results are in agreement with their data when the muscle is maximally activated, but results deviate in the resting state. Regarding TA pennation angle, the data of Maganaris and Baltzopoulos is similar to our measurements in the resting state, but deviates from our results in the maximally active state. The same inconsistent agreement with published literature is seen for *in vivo* moment arm measurements as well. The TA moment arm results reported here agree with those measured by

Maganaris (2000) using tendon excursion for both the resting and maximally active state, as Maganaris found no significant difference between moment arm measurements in the two activation states. Our results are also comparable to MRI-based moment arm measurements made by Maganaris in the same work. In contrast, Ito et al. (2000) measured the moment arm of the TA using a similar ultrasound-based tendon excursion method, finding moment arms much smaller than our measurements in the resting state, but comparable to our data in the active state. These results indicate that, while *in vivo* architecture measurement techniques offer many advantages over cadaver-based measurements, additional methodological refinement is required.

After normalizing fascicle lengths by their optimal value, the operating range of the TA was revealed to be primarily on the upper ascending limb and plateau region of the length-tension curve. Given the near doubling of measured dorsiflexion torque with increasing ankle plantarflexion found through dynamometry, and given that measured moment arms tended to decrease with increasing plantarflexion, it was expected that the TA would operate largely on the ascending limb of the length-tension curve in order to achieve such steep torque gains over the ankle range of motion. However, because the TA operating range fell near the plateau region, the range of forces the muscle was capable of generating were insufficient to match the large range of measured torque values, thus leading to disagreement with estimated joint torque. In fact, the average measured torque range was nearly 3.5 times larger than the average estimated torque range. The observed differences between estimated and measured dorsiflexion torque are consistent across subjects, indicating that a non-trivial discrepancy exists between architecture-based estimates of joint torque and measured joint torque. The cause of this discrepancy is unknown, but may include limitations in architecture measurement methods, limitations associated

with dynamometric measurements of joint torques, or perhaps current theories regarding muscle structure-function relationships are incomplete.

The influence of architecture measurement methodology and accuracy was evaluated through a series of sensitivity analyses. Recalculating estimated torque using the three described methodological variants had no significant effect on estimated torque capacity, with the exception of estimates made using scaled sarcomere lengths to account for potential deformation of muscle fibers around endoscopic probes, which were found to be significantly different from original estimates. This indicates that small variations in how the tendon excursion method is performed or the assumed value of optimal sarcomere length have minimal effect on architecture-based estimates of muscle function, but altering the value of measured sarcomere length could significantly affect torque estimates.

A sensitivity analysis performed for each measured architecture parameter revealed that functional estimates are most sensitive to sarcomere length, moderately sensitive to fascicle length and moment arm, and minimally sensitive to pennation angle. Based on the results of architecture data collection reported here and our knowledge of the computational framework used to estimate joint torque, these sensitivities make sense. Parameters that are used in early calculations, such as fascicle length and sarcomere length, which are used to calculate optimal fascicle length, tend to have a larger influence on torque estimates than do parameters used in later calculations, such as moment arm and pennation angle, which are only involved in the final step of torque calculations. Sarcomere length measurements had relatively large within-subject variability and are foundational in our functional predictions, so varying measurement values by one standard deviation altered torque estimates considerably. This large within-subject variability is likely due to challenges associated with micro-endoscopy data collection, namely the need to average

sarcomere length measurements from several different frames and probe positions because of poor image quality. In contrast, fascicle length measurements, which are also foundational to functional predictions but had lower within-subject variability, had less influence on torque estimates. Measured pennation angles had relatively low within-subject variability, and because the cosine of their value was taken, small changes had minimal impact on estimated torque. Finally, within-subject variability associated with moment arm measurements was quite high, but because moment arm is only used in the final stage of torque calculations, only moderate influence on torque estimates was observed.

A cumulative analysis, in which all parameter values and methodological choices were varied to minimize or maximize resulting torque estimates, revealed that the combined effects of all sources of influence was sufficient to explain the discrepancy between estimated and measured torque. For each subject, the range between the minimum and maximum torque curves encompassed measured torque for at least two joint position. For subjects 1, 2, and 4, measured torque fell within the range of possible torque estimates for three joint positions, and for subject 5, all four dorsiflexion torque measurements fell within the range of possible estimate values. These results indicate musculoskeletal models that estimate joint torques from muscle architecture are fairly robust to deviations from correct architecture parameter values, but the cumulative effects of these deviations can significantly alter muscle torque estimates. Thus, it is critical that methods used to measure and apply muscle architecture parameters are standardized to eliminate the influence methodological variants might have on model performance. Additionally, *in vivo* architecture measurement techniques should continue to be refined to ensure that the architecture parameters upon which models are built and validated are as accurate and consistent as possible.

5.2 Assumptions and Limitations

There were several limitations to the multi-scale *in vivo* imaging framework used throughout this study. First, fascicular architecture was measured in both the passive and active state using ultrasound; however, no method to ensure appropriate muscle activation was included in the protocol. Subjects were asked to sustain a "near maximal" contraction during active imaging, which is admittedly subjective, opening the possibility that active state architecture measurements do not sufficiently represent the architecture of the muscle during the maximum voluntary contractions associated with peak dorsiflexion torque measurements. It would have been possible to use EMG or a baseline peak force measurement to determine how close the subject was to maximal contraction during active state imaging. However, we chose not to include these steps in our protocol, as previous researchers have demonstrated that ultrasound-based measurements of fascicular architecture only vary significantly with changes in muscle activation at low activation levels (0-30%), while no significant difference exists for muscle activation changes at higher activation levels (30-100%) (Hodges et al., 2003). Because it is unlikely that subjects performed contractions as low as 30% maximal when prompted for "near maximal" contraction, we believe our active-state architecture measurements accurately represent muscle architecture during maximal voluntary contraction. Ultrasound probe orientation was also manually selected by the experimenter, which may have effected fascicle length measurements (Klimstra et al., 2007). However, architecture measurements were repeated three times under each experimental condition, so any effects due to slight off-axis probe orientations would likely average out for each condition.

There were limitations to the tendon excursion approach used to estimate the moment arm of the TA. The accuracy of the tendon excursion method has been questioned on the basis of its assumption that no tendon stretch occurs during joint rotation. Dynamic effects related to passive

joint motion could potentially lead to small levels of stretch or shortening, as could involuntary muscle activations that occur in the subject during passive joint rotation, thus invalidating this assumption. Alternative MRI-based approaches to measuring moment arm are not without their limitations (see Background), and more advanced dynamic MRI techniques were not feasible at the time this study was performed.

In addition to the limitations inherent to the tendon excursion method, there were several potential limitations to our implementation of the method. First, tendon excursion was measured with an experimenter manually moving the joint through its passive range of motion. This manual action may have varied between trials and subjects, thus presenting the opportunity for slight methodological differences between subjects. However, because passive joint motions were repeated three times for each subject and because tendon excursion data was scaled to match a pre-determined excursion-joint angle relationship, it is unlikely that slight differences in passive motion significantly affected moment arm estimates.

A final limitation to the tendon excursion approach used in this work is the fact that only peak dorsiflexion and peak plantarflexion joint positions were measured for tendon excursion; the instantaneous joint position during passive motion was not measured. It is possible that joint position did not change in precisely the same way during passive motion for each subject. Thus, using peak joint positions to scale the pre-determined excursion-joint angle relationship may have distorted the true joint dynamics for a given subject, making moment arm estimates inaccurate. Jung et al. (2015) demonstrated that using a dynamometer to measure passive range of motion is more reliable than using a handheld goniometer, as was done in this study. Ideally, tendon excursion imaging would be performed with the subject positioned in the dynamometer such that instantaneous joint position could be measured throughout passive joint motion. Unfortunately,

because of time constraints and the need for ultrasound and micro-endoscopic imaging to be performed during the same experimental session, this was not the approach used here.

On average, the moment arm data collected in this work agrees well with previously reported tendon excursion measurements of TA moment arm (Ito et al., 2000; Maganaris, 2000). Moment arms were only measured in the resting state, which is not representative of moment arm behavior during maximum voluntary contraction; however, Maganaris (2000) showed that no significant difference exists between tendon excursion estimates of moment arm in the resting and maximally active state, thus indicating that our resting state measurements are still appropriate. Some abnormalities were observed in collected moment arm data. For example, the TA moment arm of subject 2 was quite low and increased with increasing plantarflexion, which disagrees with published trends. Additionally, the moment arm of subject 5 was much higher than that of other subjects, despite subject 5's relatively small body size. These abnormalities, as well as the large within-subject standard deviations associated with moment arm measurements, indicate that perhaps the tendon excursion approach used in this study is not reliable. However, our analyses found that muscle functional estimates are only mildly sensitive to moment arm measurements relative to other parameters, despite large standard deviations observed in this work. Ultimately, based on our analyses, we do not believe inaccuracies in moment arm measurements are solely responsible for observed discrepancies between estimated and measured muscle torques.

Measurements of TA sarcomere length were limited in that they only took place at a single joint angle. It was assumed that measured fascicle length was simply the sum of a constant number of equally-sized sarcomeres, thus allowing us to estimate sarcomere length from known fascicle lengths at any joint position. This assumption would not hold true if any stretch or shortening of the TA tendon occurred as joint position was varied during fascicle length measurements.

However, we do not believe that this is the case, as sarcomeres were measured in the resting state when the tendon was slack and measured fascicle lengths agree well with published data, indicating that tendon stretch and shortening did not affect our results.

Finally, dynamometry studies are often scrutinized because it is unclear how well they are able to isolate specific muscle groups without neuromuscular effects or agonistic contributions interfering with results. To our knowledge, no research exists evaluating the activity of agonistic muscles, muscle activation potential, or motor unit recruitment across joint angles during isometric dynamometry of the ankle joint. It is possible that activation of the ankle plantarflexors reduced torque output at smaller ankle joint angles and that this antagonistic action decreased with increasing joint ankle, causing a larger increase in dorsiflexion torque with increasing plantarflexion than was predicted based on muscle architecture. It may be that maximal activation of the TA is inhibited when the joint is in dorsiflexion but not when the joint is plantarflexed. This remains a topic for future exploration. The manufacturer's dynamometry protocol was followed precisely in the present study, however, and is assumed to be accurate at this time.

Several methodological decisions were made in this study, though alternative approaches could have been used. These decisions included using a second order polynomial curve to fit tendon excursion-joint position data, assuming an optimal human sarcomere length of 2.7 μm rather than 2.8 μm, and using micro-endoscopic sarcomere lengths as measured rather than scaling measurements to account for muscle fiber deformation around the micro-endoscope probe. Evidence from published literature was used to inform each of these methodological decisions. When calculating moment arms using the tendon excursion approach, both second order and third order fit curves are used in previous studies (Ito et al., 2000; Maganaris, 2000). In this case, the second order polynomial was determined to yield results that agree slightly better with reported

TA moment arm data, so that was the primary method selected for this work. Optimal human sarcomere lengths of both 2.7 and 2.8 µm are reported in the literature, although 2.7 µm appears to be used more frequently in recent work, so that was the assumed optimal length used here (Walker and Schrodt, 1974; Woledge et al., 1985). Finally, unpublished work from Kegelman and Martin (2015) compared sarcomere lengths measured via micro-endoscopy with those measured using confocal microscopy, finding that micro-endoscopic measurements were accurate without accounting for fiber deformation around the endoscopic probe. Thus, it was determined that scaling measurements was inaccurate and unnecessary.

While all methodological decisions were evidence-based, analyses were performed in this study to explore the impact of these decisions on our results. Those analyses confirmed that, for each methodological decision described above, no significant difference was found between the results of our primary approach and the alternative approach, with the exception of scaling sarcomere lengths, which did result in torque estimates significantly different from our original estimate only at a joint position of 10° dorsiflexion. Further research is required to confirm the importance of scaling measured sarcomere lengths.

5.3 Contributions and Future Work

Several cadaver dissection studies have been performed to generate comprehensive architecture data for human musculature (Friederich and Brand, 1990; Ward et al., 2009; Wichiewicz et al., 1982). The utility of these studies is limited, however, by small sample sizes and poor agreement between cadaver muscle architecture and that of healthy living subjects (Martin et al., 2001; Van Ee et al., 2000; Vidt et al., 2011). While advancement in musculoskeletal imaging technology has enabled extensive research of *in vivo* muscle architecture, much of this data is reported in disparate studies, each focusing on a subset of architectural properties and failing to measure others

(Fukunaga, 1997; Handsfield et al., 2014). Though there are a few studies which attempt to estimate the length-tension behavior of specific muscles using *in vivo* architecture data, non-invasive *in vivo* measurements of sarcomere length were not previously available, thus raising questions regarding the validity of functional estimates made in these studies (Maganaris, 2003).

This is the first study to report comprehensive muscle architecture data *in vivo* using non-invasive biomedical imaging methods. Thus, this work is also the first in which estimates of muscle operating range and torque capacity have been derived entirely from *in vivo* muscle architecture properties. To our knowledge, this is also the only work to explore both the effect of common methodological variants across the biomechanics field and the values of *in vivo* muscle architecture parameters on theory-driven functional estimates.

In conclusion, this work describes a multi-scale imaging framework that can be used to collect comprehensive *in vivo* architecture data non-invasively in human muscle. Functional predictions derived from *in vivo* architecture data generated in this work indicate that a discrepancy exists between measured muscle torque production and architecture-based estimates of torque production. These discrepancies may be the result of limitations in the imaging techniques used, limitations of dynamometric testing to measure the isometric torque capacity of specific muscle groups, and/or limitations of the current theories relating muscle structure and function. Our sensitivity analyses indicate that functional predictions are not particularly sensitive to any individual architecture parameter value or methodological variant, but the cumulative effect of parameter sensitivity and methodological changes on torque estimates is sufficient to explain observed discrepancies between measured and estimated joint torque. Despite this result, architectural properties measured in this study largely agree with published data, indicating that it is likely a combination of the above limitations causing a breakdown between measured and

estimated muscle function. Thus, it is critical that biomechanical data collection methods continue to be improved, such that the reliability of current theories relating muscle structure and function can be adequately evaluated.

Future attention should be focused on improving imaging methods for *in vivo* muscle architecture measurement. Incorporating the latest in musculoskeletal imaging techniques, including the use of diffusion tensor MRI for studying fascicular architecture and dynamic 3D MRI for measuring muscle moment arms, would help to overcome many of the limitations associated with ultrasound-based architecture measurements and eliminate many potential sources of human error in data collection.

Another important direction for future study is to evaluate the neuromuscular activity of the muscle of interest, as well as the contributions of agonistic muscles during dynamometric testing of the ankle joint. EMG could be used to evaluate the activity of ankle plantarflexors relative to dorsiflexors during isometric testing, thus providing an indication as to whether involuntary plantarflexor activity or reduced dorsiflexor activity are inhibiting dorsiflexion moments at small ankle joint angles. This could help explain the large increase in isometric dorsiflexion torque with increasing ankle plantarflexion measured via dynamometry, which differs from the relatively steady torque estimated across the ankle range of motion that was predicted using muscle architecture measurements. To our knowledge, no previous studies have explored the activity of antagonist muscles during isometric dynamometry of the ankle joint.

Another limitation of the current work is the small sample size of five subjects. Several subjects chose to leave the study before the completion of data collection, and the micro-endoscopy portion of our protocol failed to produce usable results for other participants. Our statistical robustness is limited with n=5, and although observed trends were consistent across our five

subjects, it is possible that our results do not fully reflect the population as a whole. It is important that architecture data continue to be collected and the conclusions of this study be reevaluated.

The TA is only one of more than 300 distinct muscles in the human body, and the methods described in this work can be used to study the architecture of many of these muscles. In the future, comprehensive muscle architecture data should be collected for additional muscles with preference towards those which are most frequently the focus of musculoskeletal models and clinical disease states and therapies. This data would further shed light on the structure-function relationships of key muscle groups and help to advance biomechanical modeling technology.

REFERENCES

Arnold, E.M., Ward, S.R., Lieber, R.L. & Delp, S.L. A Model of the Lower Limb for Analysis of Human Movement. *Annals of Biomedical Engineering.* **38(2)**, 269-279 (2010).

Baker, H.B., Passipieri, J.A., Siriwardane, M., Ellenburg, M.D., Vadhavkar, M., Bergman, C.R., Saul, J.M., Tomblyn, S., Burnett, L. & Christ, G.J. Cell and Growth Factor-Loaded Keratin Hydrogels for Treatment of Volumetric Muscle Loss in a Mouse Model. *Tissue Engineering Part A.* **23**, 572-584 (2017).

Bamman, M.M., Newcomer, B.R., Larson-Meyer, D.E., Weinsier, R.L. & Hunter, G.R. Evaluation of the strength-size relationship *in vivo* using carious muscle size indices. *Medicine and Science in Sports and Exercise*. 1307-1313 (1999).

Biodex Medical Systems, Inc. System 3 Pro Application/Operation Manual.

Blemker, S.S. & Delp, S.L. Three-Dimensional Representation of Complex Muscle Architecture and Geometries. *Annals of Biomedical Engineering*. **33(5)**, 661-673 (2005).

Blemker, S.S., Asakawa, D.S., Gold, G.E. & Delp, S.L. Image-Based Musculoskeletal Modeling: Applications, Advances, and Future Opportunities. *Journal of Magnetic Resonance Imaging*. **25**, 441-451 (2007).

Boulesteix, T., Beaurepaire, E., Sauviat, M. & Schanne-Klein, M. Second-harmonic microscopy of unstained living cardiac myocytes: measurements of sarcomere length with 20-nm accuracy. *Optics Letters*. **29(17)**, 2031-2033 (2004).

Brand, R.A., Pedersen, D.R. & Friederich, J.A. The Sensitivity of Muscle Force Predictions to Changes in Physiologic Cross-Sectional Area. *Journal of Biomechanics*. **19(8)**, 589-596 (1986).

Chang, Y., Su, F., Wu, H. & An, K. Optimum length of muscle contraction. *Clinical Biomechanics*. **14**, 537-542 (1999).

Chen, X., Sanchez, G.N., Schnitzer, M.J. & Delp, S.L. Changes in sarcomere lengths of the human vastus lateralis muscle with knee flexion measured using *in vivo* microendoscopy. *Journal of Biomechanics*. **49**, 2989-2994 (2016).

Clarke, E.C., Martin, J.H., d'Entremont, A.G., Pandy, M.G., Wilson, D.R. & Herbert, R.D. A non-invasive, 3D, dynamic MRI method for measuring muscle moment arms in vivo: demonstration in the human ankle joint and Achilles tendon. *Medical Engineering & Physics.* **37(1)**, 93-99 (2015).

Cutts, A. The range of sarcomere lengths in the muscles of the human lower limb. *Journal of Anatomy*. **160**, 79-88 (1988).

Delp, S.L. & Loan, J.P. A Graphics-Based Software System to Develop and Analyze Models of Musculoskeletal Structures. *Computers in Biology and Medicine*. **25(1)**, 21-34 (1995).

Delp, S.L. & Loan, J.P. A Computational Framework for Simulating and Analyzing Human and Animal Movement. *Computing in Science and Engineering*. 46-54 (2000).

Engstrom, C.M., Loeb, G.E., Reid, J.G., Forrest, W.J. & Avruch, L. Morphometry of the human thigh muscles. A comparison between anatomical sections and computer tomographic and magnetic resonance images. *Journal of Anatomy*. **176**, 139-156 (1991).

Friederich, J.A. & Brand, R.A. Muscle Fiber Architecture in the Human Lower Limb. *Journal of Biomechanics*. **23(1)**, 91-95 (1990).

Fukunaga, T., Kawakami, Y., Kuno, S., Funato, K. & Fukashiro, S. Muscle Architecture and Function in Humans. *Journal of Biomechanics*. **30(5)**, 457-463 (1997).

Fukunaga, T., Miyatani, M., Tachi, M., Kouzaki, M., Kawakami, Y. & Kanehisa, H. Muscle volume is a major determinant of joint torque in humans. *Acta Physiologica Scandinavica*. **172**, 249-255 (2001).

Fukunaga, T., Roy, R.R., Shellock, F.G., Hodgson, J.A., Day, M.K., Lee, P.L., Kwong-Fu, H. & Edgerton, V.R. Physiological Cross-Sectional Area of Human Leg Muscles Based on Magnetic Resonance Imaging. *Journal of Orthopedic Research***. 10**, 926-934 (1992).

Gans, C. Fiber Architecture and Muscle Function. *Exercise and Sports Sciences Reviews*. **10**, 160-207 (1982).

Geboers, J.F.M., van Tuijl, J.H., Seelen, H.A.M. & Drost, M.R. Effect of Immobilization on Ankle Dorsiflexion Strength. *Scandinavian Journal of Rehabilitation Medicine*. **32**, 66-71 (2000).

Gonzalez, R.V., Buchanan, T.S. & Delp, S.L. How Muscle Architecture and Moment Arms Affect Wrist Flexion-Extension Moments. *Journal of Biomechanics*. **30(7)**, 705-712 (1997).

Gordon, A.M., Huxley, A.F. & Julian, F.J. The variation in isometric tension with sarcomere length in vertebrate muscle fibres. *The Journal of Physiology*. **184(1)**, 170-192 (1966).

Handsfield, G.G., Meyer, C.H., Hard, J.M., Abel, M.F. & Blemker, S.S. Relationships of 35 lower limb muscles to height and body mass quantified using MRI. *Journal of Biomechanics*. **47**, 631-638 (2014).

Heemskerk, A.M. & Damon, B.M. Diffusion Tensor MRI Assessment of Skeletal Muscle Architecture. *Current Medical Imaging Reviews*. **3(3)**, 152-160 (2007).

Hill, A.V. & Sec, R.S. The heat of shortening and the dynamic constants of muscle. *Proceedings of the Royal Society of London B: Biological Sciences*. **126(843)**, 136-195 (1938).

Hodges, P.W., Pengel, L.H.M., Herbert, R.D. & Gandevia, S.C. Measurement of Muscle Contraction with Ultrasound Imaging. *Muscle and Nerve*. **27**, 682-692 (2003).

Holzbaur, K.R.S., Murray, W.M., Gold, G.E. & Delp, S.L. Upper limb muscle volumes in adult subjects. *Journal of Biomechanics*. **40**, 742-749 (2007).

Inouye, J.M., Pelland, C.M., Lin, K.Y., Borowitz, K.C. & Blemker, S.S. A Computational Model of Velopharyngeal Closure for Simulating Cleft Palate Repair. *The Journal of Craniofacial Surgery.* **26(3)**, 658-662 (2015).

Ito, M., Akima, H. & Fukunaga, T. In vivo moment arm determination using B-mode ultrasonography. *Journal of Biomechanics*. **33**, 215-218 (2000).

Jung, I., Yu, I., Kim, S., Lee, D. & Oh, J. Reliability of ankle dorsiflexion passive range of motion measurements obtained using a hand-held goniometer and Biodex dynamometer in stroke patients. *Journal of Physical Therapy Sciences*. **27**, 1899-1901 (2015).

Kawakami, Y. Abe, T. & Fukunaga, T. Muscle-fiber pennation angles are greater in hypertrophied than in normal muscles. *Journal of Applied Physiology*. **74(6)**, 2740-2744 (1993).

Klimstra, M., Dowling, J., Durkin, J.L. & MacDonald, M. The effect of ultrasound probe orientation on muscle architecture measurement. *Journal of Electromyography and Kinesiology*. **17**, 504-514 (2007).

Koolmees, P.A., Korteknie, F. & Smulders, F.J.M. Accuracy and Utility of Sarcomere Length Assessment by Laser Diffraction. *Food Microstructure.* **5(1)**, 71-76 (1986).

Lieber, R.L. & Friden, J. Functional and Clinical Significance of Skeletal Muscle Architecture. *Muscle and Nerve*. **23**, 1647-1666 (2000).

Lieber, R.L., Ljung, B. & Friden, J. Intraoperative Sarcomere Length Measurements Reveal Differential Design of Human Wrist Extensor Muscles. *The Journal of Experimental Biology*. **200**, 19-25 (1997).

Lieber, R.L., Loren, G.J. & Friden, J. In Vivo Measurement of Human Wrist Extensor Muscle Sarcomere Length Changes. *Journal of Neurophysiology*. **71(3)**, 874-881 (1994).

Lieber, R.L., Yeh, Y. & Baskin, R.J. Sarcomere Length Determination Using Laser Diffraction. *Biophysical Journal*. **45**, 1007-1016 (1984).

Llewellyn, M.E., Barretto, R.P.J., Delp, S.L. & Schnitzer, M.J. Minimally invasive high-speed imaging of sarcomere contractile dynamics in mice and humans. *Nature*. **454(7)**, 784-788 (2008).

Loeb, G.E., Pratt, C.A., Chanaud, C.M. & Richmond, F.J.R. Distribution and innervation of short, interdigitated muscle fibers in parallel-fibered muscles of the cat hindlimb. *Journal of Morphology*. **191**, 1-15 (1987).

Maganaris, C.N. Force-Length Characteristics of the In Vivo Human Gastrocnemius Muscle. *Clinical Anatomy*. **16**, 215-223 (2003).

Maganaris, C.N. Force-length characteristics of *in vivo* human skeletal muscle. *Acta Physiologica Scandinavia*. **172**, 279-285 (2001).

Maganaris, C.N. Imaging-based estimates of moment arm length in intact human muscle-tendons. *European Journal of Applied Physiology*. **91**, 130-139 (2004).

Maganaris, C.N., Baltzopouls, V. & Sargeant, A.J. In vivo measurement-based estimations of the human Achilles tendon moment arm. *European Journal of Applied Physiology*. **83**, 363-369 (2000).

Maganaris, C.N. In vivo measurement-based estimations of the moment arm in the human tibialis anterior muscle-tendon unit. *Journal of Biomechanics*. **33**, 375-379 (2000).

Maganaris, C.N., Baltzopoulos, V. & Sargeant, A.J. *In vivo* measurements of the triceps surae complex architecture in man: implications for muscle function. *Journal of Physiology*. **512(2)**, 603-614 (1998).

Maganaris, C.N. & Baltzopoulos, V. Predictability of in vivo changes in pennation angle of human tibialis anterior muscle from rest to maximum isometric dorsiflexion. *European Journal of Applied Physiology*. **79**, 294-297 (1999).

Mansouri, M., Clark, A.E., Seth, A. & Reinbolt, J.A. Rectur femoris transfer surgery affects balance recovery in children with cerebral palsy: A computer simulation study. *Gait & Posture*. **43**, 24-30 (2016).

Martin, D.C., Medri, M.K., Chow, R.S., Oxorn, V., Leekam, R.N., Agur, A.M. & McKee, N.H. Comparing human skeletal muscle architectural parameters of cadavers with in vivo ultrasonographic measurements. *Journal of Anatomy*. **199**, 429-434 (2001).

Meyer, C.H., Hu, B.S., Nishimura, D.G. & Macovski, A. Fast Spiral Coronary Artery Imaging. *Magnetic Resonance in Medicine*. **28**, 202-213 (1992).

Mitsiopoulos, N., Baumgartner, R.N., Heymsfield, S.B., Lyons, W., Gallagher, D. & Ross, R. Cadaver validation of skeletal muscle measurement by magnetic resonance imaging and computerized tomomgraphy. *Journal of Applied Physiology*. (1998).

Myers, C.A., Laz, P.J., Shelburne, K.B. & Davidson, B.S. A Probabilistic Approach to Quantify the Impact of Uncertainty Propagation in Musculoskeletal Simulations. *Annals of Biomedical Engineering*. **43(5)**, 1098-1111 (2014).

Narici, M.V., Maganaris, C.N., Reeves, N.D. & Capodalgio, P. Effect of aging on human muscle architecture. *Journal of Applied Physiology*. **95**, 2229-2234 (2003).

Narici, M. Human skeletal muscle architecture studied in vivo by non-invasive imaging techniques: functional significance and applications. *Journal of Electromyography and Kinesiology*. **9**, 97-103 (1999).

Plotnikov, S.V., Millard, A.C., Campagnola, P.J. & Mohler, W.A. Characterization of the Myosin-Based Source for Second-Harmonic Generation from Muscle Sarcomeres. *Biophysical Journal*. **90**, 693-703 (2006).

Rugg, S.G., Gregor, R.J., Mandelbaum, B.R. & Chiu, L. *In Vivo* Moment Arm Calculations at the Ankle Using Magnetic Resonance Imaging (MRI). *Journal of Biomechanics*. **23(5)**, 495-501 (1990).

Sanchez, G.N., Sinha, S., Liske, H., Chen, X., Nguyen, V. Delp, S.L. & Schnitzer, M.J. In Vivo Imaging of Human Sarcomere Twitch Dynamics in Individual Motor Units. *Neuron*. **88**, 1109-1120 (2015).

Sanchez, G.N., Delp, S.L., Schnitzer, M.J. & Llewellyn, M.E. System and Method Useful for Sarcomere Imaging via Objective-Based Microscopy. *United States Patent*. Patent No. US 8897959 B2. (2014).

Steele, K.M., Seth, A., Hicks, J.L., Schwartz, M.S. & Delp, S.L. Muscle contributions to support and progression during single-limb stance in crouch gait. *Journal of Biomechanics*. **43(11)**, 2099-2105 (2010).

Thelen, D., Seth, A., Anderson, F.C. & Delp, S.L. Gait2392 lower extremity model. *OpenSim.* (2012).

Van Ee, C.A., Chasse, A.L. & Myers, B.S. Quantifying Skeletal Muscle Properties in Cadaveric Test Specimens: Effects of Mechanical Loading, Postmortem Time, and Freezer Storage. *Journal of Biomechanical Engineering*. **122** (2000).

Vidt, M.E., Daly, M., Miller, M.E., Davis, C.C., Marsh, A.P. & Saul, K.R. Characterizing upper limb muscle volume and strength in older adults: A comparison with young adults. *Journal of Biomechanics*. **45**, 334-341 (2012).

Walker, S.M. & Schrodt, G.R. I segment lengths and thin filament periods in skeletal muscle fibers of the rhesus monkey and the human. *The Anatomical Record*. **178(1)**, 63-81 (1974).

Ward, S.R., Eng, C.M., Smallwood, L.H. & Lieber, R.L. Are Current Measurements of Lower Extremity Muscle Architecture Accurate?. *Clinical Orthopaedics and Related Research*. **467**, 1074-1082 (2009).

WEIGHTTRAINIING.GUIDE. *Skeletal muscle structure.* Retrieved from https://weighttraining.guide/muscle-fibers/.

Wickiewicz, T.L., Roy, R.R., Powell, P.L. & Edgerton, V.R. Muscle Architecture of the Human Lower Limb. *Clinical Orthopaedics and Related Research*. **179**, 275-283 (1983).

Woledge, R.C., Curtin, N.A. & Homsher, E. Energetic aspects of muscle contraction. *Monographs of the Physiological Society*. **41** (1985).

Zajac, F.E. Muscle and Tendon: Properties, Models, Scaling, and Application to Biomechanics and Motor Control. *Critical Reviews in Biomedical Engineering*. **17(4)** (1989).